CCI+ PHASE 1 – NEW ECVS
PERMAFROST

CCN1 & CCN2
ROCK GLACIER KINEMATICS AS NEW ASSOCIATED PARAMETER OF ECV PERMAFROST

D4.1 Product Validation and Intercomparison Report

VERSION 1.0

27 JANUARY 2021

PREPARED BY

Document Status Sheet

Issue	Date	Details	Authors
0.1	20.10.2020	Template created based on Product Validation and Intercomparison Report of CCN 1	T. Strozzi
0.2	01.12.2020	First draft of section 2	A. Bertone
0.3	18.12.2020	Second draft all sections	L. Rouyet, A. Bertone, A. Kääb, and T. Strozzi
0.4	18.01.2020	Review	A. Kääb
0.5	25.01.2021	Review	H. Christiansen
0.6	26.01.2021	Review	R. Delaloye
1.0	27.01.2021	Final editing	A. Bartsch and A. Bertone

Author team

Aldo Bertone, Chloé Barboux and Reynald Delaloye, UNIFR

Line Rouyet and Tom Rune Lauknes, NORCE

Andreas Kääb, GUIO

Hanne H. Christiansen, UNIS

Alexandru Onaca and Flavius Sirbu, WUT

Valentin Poncos, TERRASIGNA

Tazio Strozzi and Rafael Caduff, GAMMA

Annett Bartsch, B.GEOS

ESA Technical Officer:

Frank Martin Seifert

EUROPEAN SPACE AGENCY CONTRACT REPORT

The work described in this report was done under ESA contract. Responsibility for the contents resides in the authors or organizations that prepared it.

TABLE OF CONTENTS

EXECUTIVE SUMMARY

The European Space Agency (ESA) Climate Change Initiative (CCI) is a global monitoring program that aims to provide long-term satellite-based products to serve the climate modelling and climate data user community. Permafrost has been selected as one of the Essential Climate Variables (ECVs) that are elaborated during Phase 1 of CCI+ (2018-2021). As part of the Permafrost_cci baseline project, ground temperature and active layer thickness were considered to be the primary variables that require climate-standard continuity as defined by the Global Climate Observing System (GCOS). Permafrost extent and zonation are secondary parameters, but of high interest to users. The ultimate objective of Permafrost_cci is to develop and deliver permafrost maps as ECV products primarily derived from satellite measurements. Algorithms have been identified that can provide these parameters by ingesting a set of global satellite data products (Land Surface Temperature LST, Snow Water Equivalent SWE, and Landcover) in a permafrost model scheme that computes the ground thermal regime. Annual averages of ground temperature and annual maxima of thaw depth (active layer thickness) were provided at 1 km spatial resolution during Year 1 & 2 of Permafrost_cci. The data sets were created from the analysis of lower level data, resulting in gridded, gap-free products.

In periglacial mountain environments, the permafrost occurrence is patchy, and the preservation of permafrost is controlled by site-specific conditions. Three options initiated within CCN1 and CCN2 address the need for additional regional cases in cooperation with dedicated users in characterizing mountain permafrost as local indicator for climate change and direct impact on the society in mountainous areas. Started in October 2018, CCN1 is led by a Romanian team focusing on case studies in the Carpathians. The specific objective of CCN1 is to develop and deliver maps and products for mountain permafrost, such as (i) rock glacier inventories, (ii) Rock Glacier Kinematic Time Series of selected rock glaciers and (iii) a permafrost distribution model, primarily derived from satellite measurements. Started in September 2019, CCN2 consists of two options led by Swiss and Norwegian teams focusing on the investigation and definition of a new associated ECV Permafrost product related to rock glacier kinematics. Early 2020, Rock Glacier Kinematics (RGK) has been proposed as a new product to the ECV Permafrost for the next GCOS Implementation Plan (IP). It would consist of a global dataset of surface velocity time series measured/computed on single rock glacier units. A proper rock glacier kinematics monitoring network, adapted to climate research needs, builds up a unique validation dataset for climate models for mountain regions, where direct permafrost thermal state measurements are very scarce or even lacking totally. The international Action Group on rock glacier inventories and kinematics, under the IPA (International Permafrost Association), gathering about one hundred members, supports this integration and CCN2 is working closely with this Action Group [AD-10 to AD-13]. Following the recommendations of this IPA Action Group, the overall goal of CCN2 is achieved through the development of two products: (i) regional rock glacier inventories and (ii) Rock Glacier Kinematic Time Series of selected rock glacier.

This Product Validation and Intercomparison Report (PVIR) describes the validation of the regional rock glacier inventories, the Rock Glacier Kinematic Time Series of selected rock glaciers, and the permafrost distribution model at regional scale in the Romanian Carpathians.

The validation is carried out by comparing the regional rock glacier inventories of each climatic region with available in-situ or complementary remote sensing measurements recorded at (or around) the

same temporal window. Additionally, consolidation of results on each climatic region has been achieved by the interpretation of the dataset by a second expert, in order to improve the overall quality of the inventory.

A quantitative assessment of the Rock Glacier Kinematic Time Series is performed using internal quality measures, in-situ measurements (e.g. continuous and repeated GNSS measurements) and coincident remote sensing data. The estimated accuracy of the Sentinel-1 6/12-days InSAR measurements is in the order of 0.2 mm. In the Romanian Carpathians, the quality of the multiple Sentinel-1 measurements covering overlapping periods of time between 2015-2019 and extrapolated to yearly displacement rates using the InSAR stacking technique was estimated in a least-squares sense, suggesting better than centimetric accuracy. With offset tracking of very high-resolution X-band SAR data the estimated accuracy is in the order of 0.1 m/yr. With standard normalized image cross-correlation techniques on repeat optical images a subpixel horizontal accuracy can be achieved (e.g. ±0.05 m/yr generally using images with spatial resolution of 0.4 m).

For the permafrost distribution model in the Romanian Carpathians the Area Under the Receiver Operating Curve (AUC) was used to validate the model and also to set a threshold to separate the continuous values and classify them into presence/absence of permafrost together with a confusion matrix used to validate the classification map. The validation has been performed on independent data with a spatial distribution that accounts for the imbalance of presence/absence points of the model. The AUC value for the model is AUC=0.83 and the confusion matrix for the classified model shows that 69 points (90%) out of 76 had been correctly classified.

1 Introduction

1.1 Purpose of the document

The products required within CCN1 and CCN2 of the ESA CCI project for mountain permafrost regions include (i) regional kinematics-based rock glaciers inventories (RGI), (ii) Rock Glacier Kinematic Time Series (RGK) on selected rock glaciers, and (iii) a mountain permafrost distribution model (MPDM) in the Carpathians. The Product Validation and Intercomparison Report (PVIR) describes the validation using independent measurements, according to the approach introduced in the PVP [RD-27].

1.2 Structure of the document

Section 2 provides the validation of the rock glaciers inventories.

Section 3 describes the validation of the Rock Glacier Kinematic Time Series on selected rock glaciers, including the trends in rock glaciers velocity in the Romanian Carpathians.

Section 4 describes the validation of the permafrost distribution model at regional scale in the Romanian Carpathians.

1.3 Applicable documents

[AD-1]   ESA 2017: Climate Change Initiative Extension (CCI+) Phase 1 – New Essential Climate Variables - Statement of Work. ESA-CCI-PRGM-EOPS-SW-17-0032

[AD-2]   Requirements for monitoring of permafrost in polar regions - A community white paper in response to the WMO Polar Space Task Group (PSTG), Version 4, 2014-10-09. Austrian Polar Research Institute, Vienna, Austria, 20 pp

[AD-3]   ECV 9 Permafrost: assessment report on available methodological standards and guides, 1 Nov 2009, GTOS-62

[AD-4]   GCOS-200. 2016. The Global Observing System for Climate: Implementation Needs. GCOS Implementation Plan, WMO

[AD-5]   GEO/CEOS Quality Assurance framework for Earth Observation (QA4EO) protocols 3-4

[AD-6]   ESA Climate Change Initiative. CCI Project Guidelines. EOP-DTEX-EOPS-SW-10-0002

[AD-7]   National Research Council. 2014. Opportunities to Use Remote Sensing in Understanding Permafrost and Related Ecological Characteristics: Report of a Workshop. Washington, DC: The National Academies Press. https://doi.org/10.17226/18711.

[AD-8]   IPA Action Group 'Specification of a Permafrost Reference Product in Succession of the IPA Map' (2016): Final report. https://ipa.arcticportal.org/images/stories/AG_reports/IPA_AG_SucessorMap_Final_2016.pdf

[AD-9]   GlobPermafrost team (2017): Summary report from 3rd user Workshop. ESA DUE GlobPermafrost project. ZAMG, Vienna.

https://www.globpermafrost.info/cms/documents/reports/ESA_DUE_GlobPermafrost_workshop_summary_ACOP_v1_public.pdf

[AD-10] IPA Action Group Rock glacier inventories and kinematics, 2020. Towards standard guidelines for inventorying rock glaciers. Baseline concepts. Last version available on https://bigweb.unifr.ch/Science/Geosciences/Geomorphology/Pub/Website/IPA/CurrentVersion/Current_Baseline_Concepts_Inventorying_Rock_Glaciers.pdf

[AD-11] IPA Action Group Rock glacier inventories and kinematics, 2020. Kinematics as an optional attribute of standardized rock glacier inventories. Last version available on: https://bigweb.unifr.ch/Science/Geosciences/Geomorphology/Pub/Website/IPA/CurrentVersion/Current_KinematicalAttribute.pdf

[AD-12] IPA Action Group Rock glacier inventories and kinematics, 2020. Rock glaciers kinematics as an associated parameter of ECV Permafrost. Last version available on: https://bigweb.unifr.ch/Science/Geosciences/Geomorphology/Pub/Website/IPA/CurrentVersion/Current_RockGlacierKinematics.pdf

[AD-13] IPA Action Group Rock glacier inventories and kinematics, 2020. Response to GCOS ECV review – ECV Permafrost. ECV Product: Rock Glacier Kinematics. Available on: https://gcos.wmo.int/en/ecv-review-2020.

[AD-14] Rock glacier inventory using InSAR (kinematic approach). Available on: https://bigweb.unifr.ch/Science/Geosciences/Geomorphology/Pub/Website/CCI/CurrentVersion/Current_InSAR-based_Guidelines.pdf

1.4 Reference Documents

[RD-1] A. Bartsch, H. Matthes, S. Westermann, B. Heim, C. Pellet, A. Onaca, C. Kroisleitner, T. Strozzi: ESA CCI+ Permafrost User Requirements Document (URD), v1.1 12 February 2019

[RD-2] A. Bartsch, S. Westermann, T. Strozzi, A. Wiesmann, C. Kroisleitner: ESA CCI+ Permafrost Product Specifications Document (PSD), v2.0 30 November 2019

[RD-3] A. Bartsch, S. Westermann, B. Heim, M. Wieczorek, C. Pellet, C. Barboux, C. Kroisleitner, T. Strozzi: ESA CCI+ Permafrost Data Access Requirements Document (DARD), v1.0 15 January 2019

[RD-4] A. Bartsch, S. Westermann, T. Strozzi: ESA CCI+ Permafrost Product Validation and Algorithm Selection Report (PVASR), v2.0 30 November 2019

[RD-5] S. Westermann, A. Bartsch, T. Strozzi: ESA CCI+ Permafrost Algorithm Theoretical Basis Document (ATBD), v2.0 30 November 2019

[RD-6] S. Westermann, A. Bartsch, B. A. Heim, T. Strozzi: ESA CCI+ Permafrost End-to-End ECV Uncertainty Budget (E3UB), v2.0 30 November 2019

[RD-7] S. Westermann, A. Bartsch, B. A. Heim, T. Strozzi: ESA CCI+ Permafrost Algorithm Development Plan (ADP), v2.0 30 November 2019

[RD-8] B. Heim, M. Wieczorek, C. Pellet, R. Delaloye, C. Barboux, S. Westermann, A. Bartsch, T. Strozzi: ESA CCI+ Permafrost Product Validation Plan (PVP), v2.0 30 November 2019

[RD-9] A. Wiesmann, A. Bartsch, S. Westermann, T. Strozzi: ESA CCI+ Permafrost System Requirement Document (SRD), v2.0 29 February 2020

[RD-10] A. Wiesmann, A. Bartsch, S. Westermann, T. Strozzi: ESA CCI+ Permafrost System Specification Document (SSD), v2.0 29 February 2020

[RD-11] A. Wiesmann, A. Bartsch, S. Westermann, T. Strozzi: ESA CCI+ Permafrost System Verification Report (SVR), v2.0 31 May 2020

[RD-12] B. Heim, M. Wieczorek, C. Pellet, R. Delaloye, A. Bartsch, D. Jakober, G. Pointner, T. Strozzi, GAMMA: ESA CCI+ Permafrost Product Validation and Intercomparison Rerport (PVIR), v2.0 30 September 2020

[RD-13] J. Obu, S. Westermann, T. Strozzi, A. Bartsch.: ESA CCI+ Permafrost Climate Research Data Package Version 1 (CRDPv1), v2.0 31 May 2020

[RD-14] A. Bartsch, J. Obu, S. Westermann, T. Strozzi: ESA CCI+ Permafrost Product User Guide (PUG), v2.0 27 May 2020

[RD-15] I. Nitze, G. Grosse, B. Heim, M. Wieczorek, H. Matthes, A. Bartsch, T. Strozzi: ESA CCI+ Permafrost Climate Assessment Report (CAR), v2.1 16 October 2020

[RD-16] T. Strozzi, A. Onaca, V. Poncos, F. Ardelean, A. Bartsch: ESA CCI+ Permafrost CCN1 D1. User Requirement, Product Specifications and Data Access Requirements Document, v1.0 15 February 2019

[RD-17] A. Onaca, F. Ardelean, F. Sirbu,V. Poncos, T. Strozzi, A. Bartsch: ESA CCI+ Permafrost CCN1 D2. Algorithm Development Document, v1.0 31 May 2019

[RD-18] A. Wiesmann, T. Strozzi, A. Onaca, F. Sîrbu, A. Bartsch: ESA CCI+ Permafrost CCN1 D3. System Development Document, v1.0 30 September 2019

[RD-19] F. Sîrbu, A. Onaca, V. Poncos, T. Strozzi, A. Bartsch: ESA CCI+ Permafrost CCN1 D4. Product Generation and Validation Document, v1.0 30 April 2020

[RD-20] F. Sîrbu, A. Onaca, V. Poncos, T. Strozzi, A. Bartsch: ESA CCI+ Permafrost CCN1 D5. Climate Assessment Report, v1.0 30 November 2020

[RD-21] C. Barboux, A. Bertone, R. Delaloye, A. Onaca, F. Ardelean, V. Poncos, A. Kääb, L. Rouyet, H. H. Christiansen, T. Strozzi, A. Bartsch: ESA CCI+ Permafrost. CCN1 & CCN2 Rock Glacier Kinematics as New Associated Parameter of ECV Permafrost. D1.1 User Requirement Document (URD), v1.0 30 November 2019

[RD-22] C. Barboux, A. Bertone, R. Delaloye, A. Onaca, F. Ardelean, V. Poncos, A. Kääb, L. Rouyet, H. H. Christiansen, T. Strozzi, A. Bartsch: ESA CCI+ Permafrost. CCN1 & CCN2 Rock Glacier Kinematics as New Associated Parameter of ECV Permafrost. D1.2 Product Specification Document (PSD), v1.0 30 November 2019

[RD-23] C. Barboux, A. Bertone, R. Delaloye, A. Onaca, F. Ardelean, V. Poncos, A. Kääb, L. Rouyet, H. H. Christiansen, T. Strozzi, A. Bartsch: ESA CCI+ Permafrost. CCN1 & CCN2 Rock Glacier Kinematics as New Associated Parameter of ECV Permafrost. D1.3 Data Access Requirement Document (DARD), v1.0 30 November 2019

[RD-24] L. Rouyet, T. R. Lauknes, C. Barboux, A. Bertone, R. Delaloye, A. Kääb, H. H. Christiansen, A. Onaca, F. Sirbu, V. Poncos, T. Strozzi, A, Bartsch: ESA CCI+ Permafrost.

CCN1 & CCN2 Rock Glacier Kinematics as New Associated Parameter of ECV Permafrost. D2.1 Product Validation and Algorithm Selection Report (PVASR), v1.0 April 30, 2020

[RD-25] L. Rouyet, T. R. Lauknes, C. Barboux, A. Bertone, R. Delaloye, A. Kääb, H. H. Christiansen, A. Onaca, F. Sirbu, V. Poncos, T. Strozzi, A, Bartsch: ESA CCI+ Permafrost. CCN1 & CCN2 Rock Glacier Kinematics as New Associated Parameter of ECV Permafrost. D2.2 Algorithm Theoretical Basis Document (ATBD), v1.0 April 30, 2020

[RD-26] L. Rouyet, T. R. Lauknes, C. Barboux, A. Bertone, R. Delaloye, A. Kääb, H. H. Christiansen, A. Onaca, F. Sirbu, V. Poncos, T. Strozzi, A, Bartsch: ESA CCI+ Permafrost. CCN1 & CCN2 Rock Glacier Kinematics as New Associated Parameter of ECV Permafrost. D2.3 End-to-End ECV Uncertainty Budget (E3UB), v1.0 April 30, 2020

[RD-27] L. Rouyet, T. R. Lauknes, C. Barboux, A. Bertone, R. Delaloye, A. Kääb, H. H. Christiansen, A. Onaca, F. Sirbu, V. Poncos, T. Strozzi, A, Bartsch: ESA CCI+ Permafrost. CCN1 & CCN2 Rock Glacier Kinematics as New Associated Parameter of ECV Permafrost. D2.4 Algorithm Development Plan (ADP), v1.0 April 30, 2020

[RD-28] L. Rouyet , T. Rune Lauknes, C. Barboux, A. Bertone, R. Delaloye, A. Kääb, H. H. Christiansen, A. Onaca, F. Sirbu, V. Poncos, T. Strozzi, A, Bartsch: ESA CCI+ Permafrost. CCN1 & CCN2 Rock Glacier Kinematics as New Associated Parameter of ECV Permafrost. D2.5 Product Validation Plan (PVP), v1.0 April 30, 2020

[RD-29] A. Wiesmann, T. Strozzi: ESA CCI+ Permafrost. CCN1 & CCN2 Rock Glacier Kinematics as New Associated Parameter of ECV Permafrost. System Specification Document (SSD), v1.0 30 November 2020

[RD-30] A. Bertone, C. Barboux, R. Delaloye, L. Rouyet, T. Rune Lauknes, A. Kääb, H. H. Christiansen, A. Onaca, F. Sirbu, V. Poncos, R. Caduff, T. Strozzi, A, Bartsch: ESA CCI+ Permafrost. CCN1 & CCN2 Rock Glacier Kinematics as New Associated Parameter of ECV Permafrost. D4.2 Climate Research Data Package (CRDP), v1.0 23 December 2020

[RD-31] A. Bertone, C. Barboux, R. Delaloye, L. Rouyet, T.R. Lauknes, A. Kääb, H. H. Christiansen, A. Onaca, F. Sirbu, V. Poncos, T. Strozzi, R. Caduff and A. Bartsch, 2020: ESA CCI+ Permafrost. CCN1 & CCN2 Rock Glacier Kinematics as New Associated Parameter of ECV Permafrost. D4.3 Product User Guide (PUG), v1.0 23 December 2020

1.5 Bibliography

A complete bibliographic list that supports arguments or statements made within the current document is provided in Section 5.1.

1.6 Acronyms

A list of acronyms is provided in Section 5.2.

1.7 Glossary

A comprehensive glossary of terms relevant for the parameters addressed in Permafrost_cci is available as part of the User Requirement Documents of the baseline project [RD-1] and of CCN 1-2 [RD-21].

2 Regional Rock Glaciers Inventories

2.1 Methods for quality assessment

The performance of the methodology for the kinematic rock glacier inventory was assessed in an "inter-comparison" exercise. During this exercise, the partners applied the guidelines [RD-14] on the same region during a workshop held in February 2020 in Fribourg (Switzerland). The results were collected and discrepancies between different operators were evaluated to assess the homogeneity in between partners. Guidelines were refined accordingly. Furthermore, as the aim is to provide homogeneous RGIs, the practical exercise allowed to learn the standardized methodology and to get familiar with the guidelines.

Subsequently, the refined guidelines were applied on the climatic regions. To ensure a high quality of RGIs, two steps were followed on each climatic region: as first step assessment of results, and as second step consolidation of results.

The first step of assessment of results has been achieved by comparing the inventoried moving areas of each climatic region with available in-situ or complementary remote sensing measurements recorded at (or around) the same temporal frame. Pre-existing inventories of slope movements (landslide and/or rock glaciers), terrestrial geodetic survey data (DGPS, total station, lidar, etc.), as well as air-borne photogrammetry data were used, when existing, to assess the quality of the results. In the absence of terrestrial data, only the analysis of several interferograms and a good knowledge of the corresponding geomorphology allow the signal to be interpreted as a movement and not attributed to noise or atmospheric artefacts. However, the presence of a clear signal on a wider time interval, which confirms the activity of the landform, is an absolute prerequisite for attributing the signal to a geomorphodynamic displacement rather than to noise. Furthermore, the inter-comparison with other remote sensing or in-situ data may be performed to verify that the documented rock glacier unit falls into the correct category (order of magnitude of the mean velocity).

The second step of consolidation of results for each climatic region has been achieved by the interpretation of the dataset by a second operator, to improve the overall reliability of the inventory. Moving areas and kinematic attributes are assigned by the first operator, who also provides the reliability degrees. Then, the second operator checks the results of the first operator, confirming the results or modifying them. In addition, the first operator can also suggest supplementary checks at the second operator assignments for specific cases. The uncertainties are reduced by taking advantage of the knowledge of two different operators. At least two persons perform the work to reduce operator's subjectivity and ensure best quality of the results.

2.2 Inter-comparison exercise

2.2.1 Reference data

The "inter-comparison" exercise was conducted on two regions named "Arolla" and "Rechy", both located in the Western Swiss Alps (Figure 2.2.1). On Rechy both ascending and descending geometries were provided. On Arolla only descending geometry was provided, due to the overall westward slope orientation of this area. Several wrapped interferograms generated with different sensors (e.g. ALOS-2, COSMO-SkyMed, TerraSAR-X, and Sentinel-1) and with different time intervals were provided for different periods of time. Displacement information was also provided,

through (i) displacement maps obtained by stacking all the consecutive interferograms, and (ii) displacement rates measured for particular points by the persistent scatter technique.

During the exercise, the partners outlined the moving areas and compiled the fields in the attribute table of each detected polygon, following the guidelines. Then, the rock glaciers (previously identified) were characterized by filling the fields in the attribute table. The collected results (e.g. outlines and velocity classes of moving area, and kinematic classes of rock glacier) were analysed and discrepancies between different operators were evaluated to assess the homogeneity between partners.
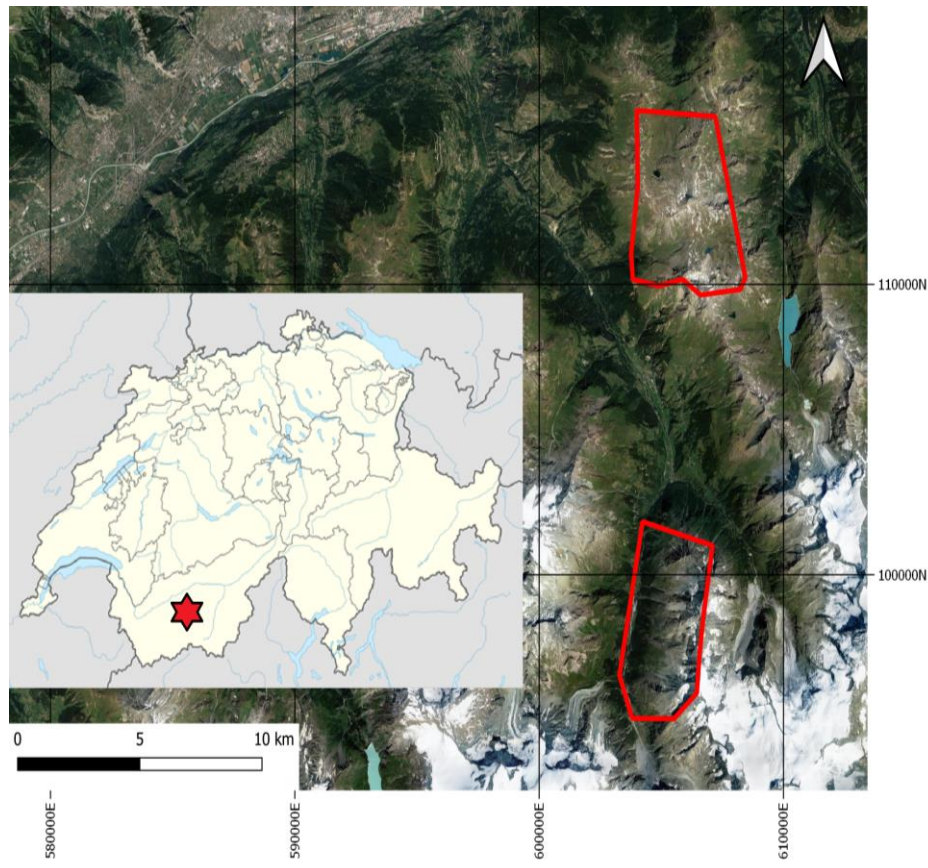

Figure 2.2.1: Location of the two regions where the rock glacier inventory inter-comparison exercise was conducted. Red star is the location of the regions on the Western Swiss Alps. The red polygon to the north outlines the Rechy region, the red polygon to the south outlines the Arolla region.

2.2.2 Match up analyses

The following analyses were conducted on 12 sites within the selected regions, investigated by all partners, where the moving areas are related to rock glaciers.

The first analysis conducted consisted in evaluating whether the surface extension of the moving areas mapped for each site is homogeneous among all partners. The evaluation results are presented with boxplots in Figure 2.2.2. For each study site, the boxplot shows the distribution of the surface extension of the moving areas mapped by all operators. Results suggest that, for each study site, the surface extensions of the moving areas outlined by all operators are similar, except for the sites 2 and 9. The reason for explaining the discrepancies in the latter two sites appears to be the large temporal- and spatial- variations in velocity, which makes the signal more difficult to interpret. The signal can

therefore be interpreted in different ways, considerably increasing the variability of the surface extension.
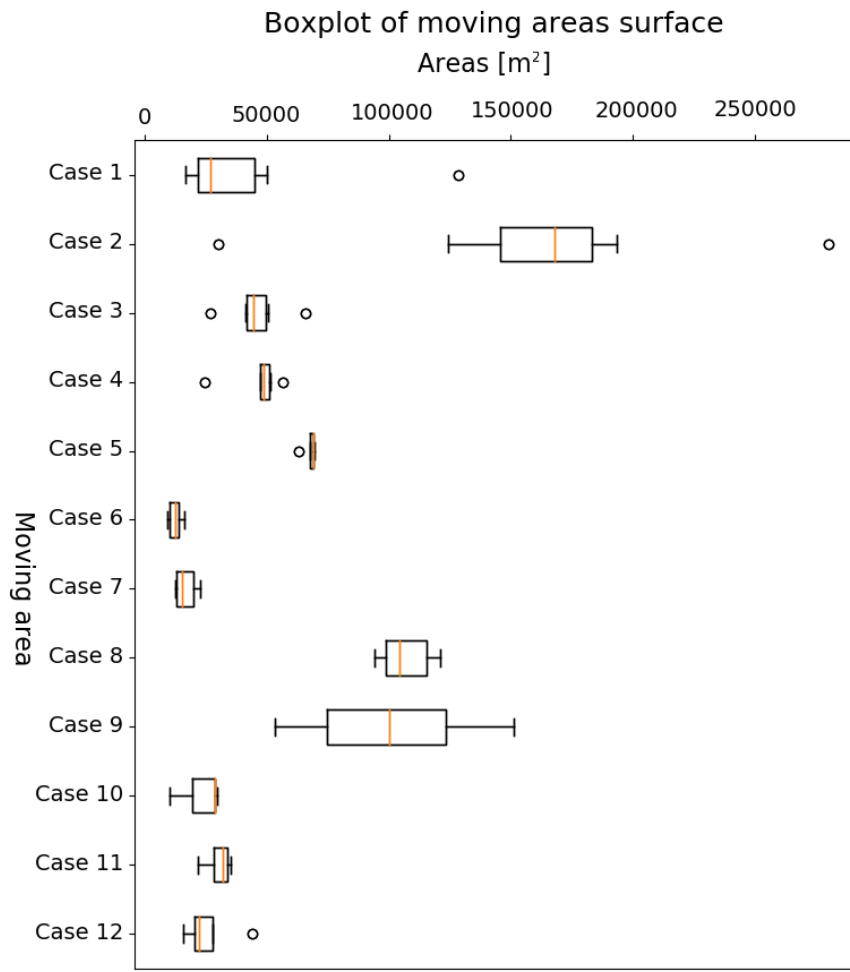

Figure 2.2.2: Boxplots of the distribution of the surface extension of each moving area mapped by all operators for each study site. Circles represent the outliers.

The second part of the analysis consisted in evaluating the homogeneity of the classification, e.g. (i) if the same moving areas was classified with the same velocity classes by all partners, and (ii) if the same rock glacier has been classified with the same kinematic classes by all partners. The evaluation is presented in Figure 2.2.3. For each study site, the upper bar (e.g. RG) shows the number of kinematic classes attributed by all operator to the same rock glacier. The lower bar (e.g. MA) shows the number of velocity classes assigned by all operators to the same moving area.

Looking at the results of moving areas, three moving areas (sites 7, 8 and 9) were classified using two categories of velocity classes. Seven moving areas (sites 2, 3, 4, 5, 6, 10 and 12) were classified using three categories of velocity classes. Two moving area (sites 1 and 11) were classified using four categories of velocity classes. Only two moving area sites are therefore classified using four categories of velocity classes. The reason for explaining the discrepancies in these sites again seems to be the large temporal- and spatial- variations in velocity, which greatly increases the uncertainty of the velocity classification. Ten moving areas are classified using two or three categories of velocity

classes. In most study sites, the same moving area is therefore classified with similar and consecutive velocity classes, ensuring reliable homogeneity in the classification.

Looking at the results of rock glaciers, two rock glaciers (sites 7 and 9) were classified using two categories of kinematic classes, seven rock glaciers (sites 1, 3, 5, 6, 8, 11 and 12) were classified using three categories of kinematic classes, two rock glaciers (sites 4 and 10) were classified using four categories of kinematic classes, and one rock glacier (site 2) was classified using five categories of kinematic classes. Three rock glaciers are therefore classified using four or five categories of kinematic classes. Nine rock glaciers are classified using two or three categories of kinematic classes. In most sites, the same rock glacier is classified with similar and consecutive kinematic classes, ensuring a fair homogeneity in the classification.

In the study sites 1, 2, 3, 4, 5, 6, 10, 11 and 12 some partners have identified more than one moving area related to the rock glacier. This is also visible in Figure 2.2.3, because the number of moving areas is greater than the number of rock glaciers. The "translation rules" from the moving area's velocity classes to the rock glacier's kinematic classes are described in the guidelines [RD-33]. However, the results suggest greater discrepancies in the kinematic classification of the rock glaciers compared to the velocity classification of the moving area. One possible reason seems to be the great velocity heterogeneity of the moving areas related to the rock glaciers, which makes it more difficult to assign the kinematic attribute to the rock glacier.

Figure 2.2.3 shows that the assignment of classes is less variable between operators when the velocity is higher. This is probably due to the wider velocity range of the fastest classes, compared to the slower classes where the velocity range of each class is smaller. Consequently, the faster the movement, the greater the reliability of the classification.

The "inter-comparison" exercise suggested the presence of particular discrepancies for some specific sites. For example, the greater discrepancies were observed when the velocity variation in the moving areas is very large, when the extent of the moving areas is very different from the geomorphological outline of the rock glacier, or when two or more moving areas with different velocity classes are related to the same rock glacier. The problems and discrepancies identified are therefore related to the lack of detailed information in the guidelines for specific sites. This lack of information leaves the operator greater freedom of decision, increasing subjectivity, and consequently the discrepancies and uncertainties detected. Therefore, to solve these detected problems, specific additional technical notes have been developed and included in the current guidelines [RD-33].
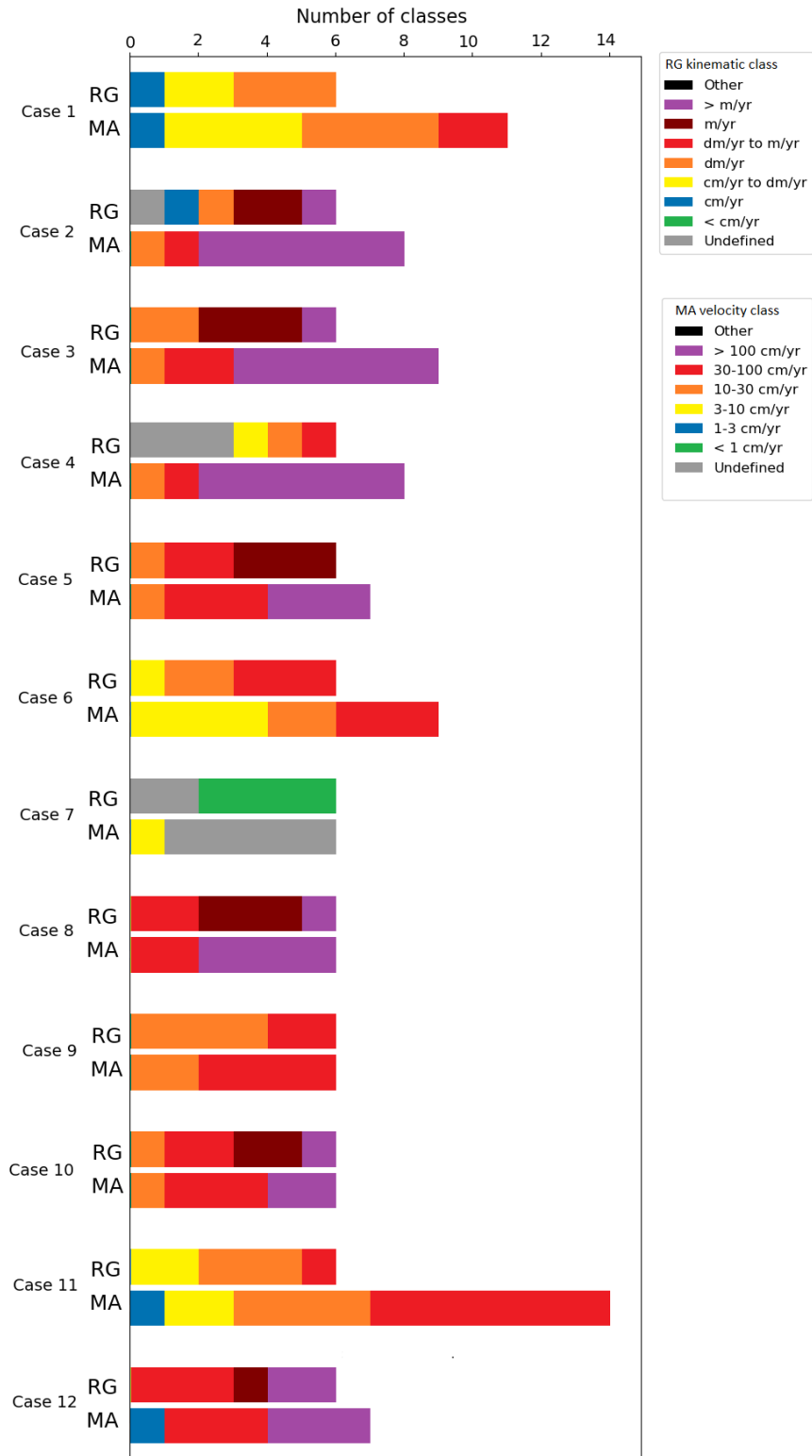
Figure 2.2.3: Horizontal bars of kinematic classes and velocity classes for the 12 study sites. For each site study, the upper bar (e.g. RG) shows the number of kinematic classes with which the same rock glacier has been classified by all operators. The lower bar of each study site (e.g. MA) shows the number of velocity classes with which the same moving area has been classified by all operators.

2.3 Results of the assessment on the available geographical regions

2.3.1 Validation for the Swiss Alps study area

In the Swiss Western Alps, the identification and characterization of moving areas and rock glaciers have been processed manually, using multiple temporal InSAR interferograms. The mapping was restricted to sites covered by rock glaciers. Some rock glaciers are monitored using in-situ measurements (e.g. GNSS). Here, a semi-quantitative evaluation is proposed to compare the moving area velocities and rock glacier kinematic attributes with the data from in-situ measurements during the same time frame.

On 7 rock glaciers, GNSS data acquired in summers 2018 and 2019 are available. These rock glaciers are described below, and the velocities detected by InSAR in summers 2018 and 2019 are compared with the 3D GNSS measurements during the same time frame.

The Petit Vélan rock glacier (Figure 2.3.1.1a) may be considered as partially destabilized since around 1995. Following the opening of a transversal crevasse about 200m above the front, the terminal tongue was gradually separating itself from the main rock glacier body and started to move at several meters per year before to dramatically decelerate since 2015. Annual velocity measurements of the rock glacier have been carried out by GNSS since 2005. During the summers (from July to October) 2018 and 2019, GNSS measured 3D velocities around 0.69-1.43 m/yr (summer 2018) and 0.73-2.02 m/yr (summer 2019) in the intact part (upper part), and 1.02-2.22 m/yr (summer 2018) and 0.67-1.69 m/yr (summer 2019) in the destabilized part (lower part). Furthermore, few points in the central axis of the moving part are still moving significantly fast, else is much less (5-10 cm/yr). With InSAR data two moving areas were mapped, with velocity classes of 30-100 cm/yr (in the lower part) and >100 cm/yr (in the upper part). The rock glacier was classified by distinguishing three units, whose kinematics were defined respectively as "dm/yr to m/yr" for one unit and "m/yr or higher" for two uppermost units.

On the Mille rock glacier, GNSS measurements indicate that it is still moving at a few centimetres per year in spite of its inactive appearance. During the 2018-2019 period, GNSS measured velocities around 2.5 – 3.5 cm/yr. With InSAR data a moving area was mapped, with velocity class of 1-3 cm/yr. The rock glacier was classified as "cm/yr".

The small active rock glacier Lapires moves at a speed of 50 cm to more than one meter per year, but the summer velocity (from July to October) is about 60-80% faster than the annual velocity. During the 2018-2019 period, GNSS measured annual velocities around 0.75 – 0.8 m/yr, but summer velocities as high as 1.5 m/yr in 2018 (not measured in 2019). With InSAR data a moving area was mapped, with a velocity class of >100 cm/yr. The rock glacier was classified as "m/yr or higher".

The rock glacier located at the eastern slopes of Mont de l'Etoile moved at several meters per year around 1995. GNSS measurements, which have been performed between 2013 and 2018, have indicated velocities of 5-7 m/yr, decreasing over time. During the last investigated period (2017-2018), GNSS measured velocities of 1.3 m/yr in the upper part, and 1.9 m/yr in the lower part. With InSAR data two moving areas were mapped, with velocity classes of 30-100 cm/yr (in the lower part) and >100 cm/yr (in the upper part). The rock glacier was classified by distinguishing two units, whose kinematics were defined respectively as "dm/yr to m/yr" and "m/yr or higher".

On the Tsarmine rock glacier the displacement measurements started in 2004 and show velocities of several meters per year. During the 2018-2019 period, GNSS measured annual velocities between 2.5

and 11 m/yr, with summer velocities being close to the annual mean. With InSAR data a moving area with velocity class of >100 cm/yr was mapped. The rock glacier was classified as "m/yr or higher".

The displacement of Tsavolire (La Tsevalire) rock glacier (Figure 2.3.1.1b) has been monitored from 2013 onwards with a permanent GNSS station. During the 2018-2019 period, GNSS measured 3D summer velocities around 1.0 (+/-0.1) m/yr. With InSAR data a moving area was mapped, with velocity class of >100 cm/yr. The rock glacier was classified as "m/yr or higher".

The last site is the Becs-de-Bosson rock glacier (Figure 2.3.1.1c). The deformation field of the rock glacier is of a complex nature. Maximum speeds locally exceeded two meters per year for instance between 2013 and 2017 while the main front moved only a few centimetres. During the 2018-2019 period, GNSS permanent stations in the faster area measured summer velocities by 2.0 (+/- 0.8) m/yr, whereas a GNSS survey revealed 4-12 cm/yr of displacement in the terminal section. With InSAR data two moving areas were mapped, the largest one located in the main body of the rock glacier with a velocity class of >100 cm/yr, and the smaller one located in the frontal part with a velocity class of 3-10 cm/yr. The rock glacier was classified by distinguishing two units, whose kinematics were defined as "m/yr or higher" for both.

For three rock glaciers, InSAR kinematic attributes fall into the correct category according to GNSS measurements. For four landforms, there is a (partial) mismatch between the GNSS and InSAR measurements of some units. The Petit Vélan rock glacier was classified by distinguishing three units, but one unit was classified as "dm/yr to m/yr" by InSAR, despite the GNSS-measured velocity is higher than m/yr. This underestimation is probably related to a relatively slow velocity around a tiny central area, that reduces the general velocity detected with InSAR. For the same reason, also the velocity class of the moving area in the lower part was underestimated. Similar is also the Mont de l'Etoile rock glacier, where one unit was underestimated with InSAR, probably because of the differences between the orientation of the real 3D displacement detected by GNSS and the orientation of the projected displacement along the LOS. The same reason can also explain the underestimation of the moving area velocity class. For Lapires rock glacier the difference is inversed (0.75 – 0.8 m/yr of GNSS movement and "m/yr or higher" of InSAR-based kinematics). This rock glacier is characterized by strong inter-annual velocity variations, with summer velocity (from July to October) about 60-80% faster than the annual velocity. The moving area was correctly classified (>1.5 m/yr of GNSS movement and ">100 cm/yr" of InSAR-based velocity class, both detected in summer periods) but the conversion into annual velocity to assign the kinematic attribute to the rock glacier unit introduces an overestimation because of the strong velocity reduction in winter periods. In Becs-de-Bosson GNSS measurements are in agreement with the two moving areas velocity classes, but in disagreement with one of the two rock glaciers kinematic attributes. However, this mismatch in one unit is related to the predominance of the moving area with ">100 cm/yr" velocity class on most of the unit's surface, compared with the more restricted moving area with "3-10 cm/yr" velocity class.

Overall, 8 out of 11 rock glacier units are correctly classified, which is considered as a good proportion considering the differences of measurement properties (punctual vs spatial distributed), the LOS-dependent measurements and the large velocity heterogeneity in time. Better agreements are obtained comparing the moving area velocity classes with the summer GNSS velocities. 8 of 10 moving areas are correctly classified because both InSAR and GNSS measurements cover the same (summer) periods.
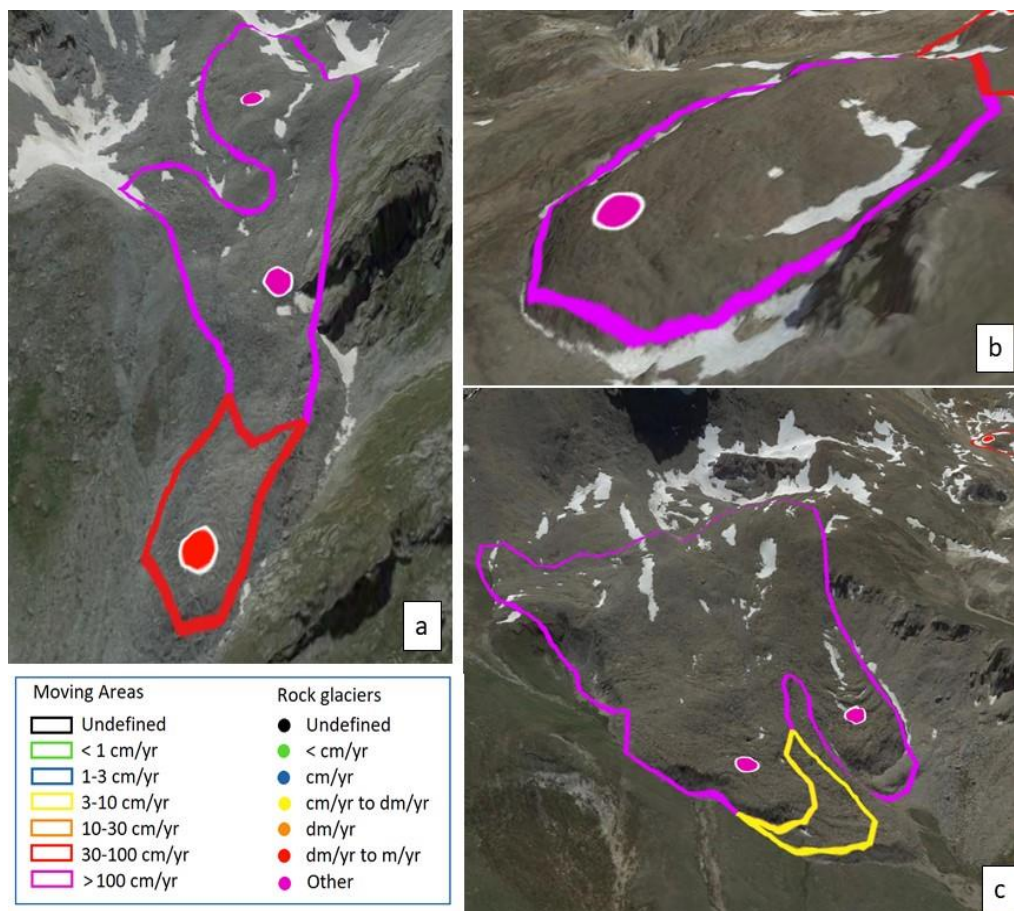
Figure 2.3.1.1: Velocities of moving areas and the entire rock glaciers of the Petit Vélan rock glacier (a), Tsavolire rock glacier (b) and Becs-de-Bosson rock glacier (c).

2.3.2 Validation of the Norwegian study areas

In Troms (study area 7), Finnmark (study area 8) and Svalbard (study area 9) Sentinel-1 data have been processed using a multiple temporal InSAR stacking procedure, consisting of averaging several unwrapped interferograms with five complementary ranges of temporal intervals between acquisitions, and then classifying the velocity results according to the common standards. This allows mapping the whole region, also in areas not covered by rock glaciers. This is valuable in regions where no extensive validation dataset on rock glacier landforms, but where in-situ measurements are available on other landform types (e.g. rockslides in Troms, solifluction sheets in Svalbard). Here we present/propose a preliminary and semi-quantitative evaluation of the moving area velocities and rock glacier kinematic attributes compared to data from other studies and in-situ measurements. This work is still on-going. On the mainland, the independently processed PSI-based open-access Norwegian Ground Motion Mapping Service (InSAR Norway, NGU, 2020; Dehls et al., 2019) also allows for comparing the results, especially for the 3–4 first velocity classes (<0.3, 0.3–1, 1–3, 3–10 cm/yr). Both in Troms and Finnmark, the CCI results are overall consistent with InSAR Norway.

In Troms, when looking at the distribution of the results in the whole study area (Figure 2.3.2.1), clusters of moving areas are detected, for example on the Njárgavárri/Badjánvárri mountain slope along Kåfjorddalen (Figure 2.3.2.1, lower-right inset) and over the Ádjet mountain slope along

Skitbotndalen (Figure 2.3.2.1, upper-left inset), where the moving areas match the delineation of the rock glacier inventory based on morphological criteria. In Njárgavárri, this is especially clear for a large rock glacier complex homogenously documented with 10–30 cm/yr velocity class (dm/yr kinematic attribute). This area has also been documented by Eriksen et al. (2017a), who measured similar velocity ranges using another satellite sensor (TerraSAR-X) and another processing technique (2D InSAR). In Ádjet, the velocity is more than 30 cm/yr at several locations. Over two initially inventoried rock glaciers, the class "Decorrelated" covers the frontal parts of the lobes, highlighting that these areas are moving over the threshold of 85 cm/yr (m/yr kinematic attribute). These rock glaciers have been studied in detail by Eriksen et al. (2018), who evidenced similar findings with a combination of different remote sensing methods (optical and radar, satellite and terrestrial).

Permanent or periodic monitoring of rockslides for societal safety reasons within the study area provides comparable data over 20 landforms. Two well-known rockslides are documented by cm/yr and cm–dm/yr kinematics in the study: 1) Gámánjunni 3 (in Manndalen) and 2) Jettan (along Storfjord) (Figure 2.3.2.2). These are two high-risk objects continuously monitored, for which the InSAR-based categorization fits with monitoring data (mostly 3–10 cm/yr for Gámánjunni 3; mostly 1–3 cm/yr for Jettan) (Blikra et al., 2009; 2015; Böhme et al., 2016; 2019; Eriksen et al., 2017b). For 18 other rockslides, periodic GNSS data are available. Based on the open-access InSAR Norway, an additional velocity class (0.1–0.3 cm/yr) has been added to document slow-moving rock slope deformation. For 13 cases, InSAR kinematics falls into the correct category according to GNSS measurements. Three landforms are not comparable (undefined InSAR-based kinematics). For two landforms, there is a mismatch between the GNSS and InSAR measurements. One of them have < 0.1 cm/yr InSAR-based kinematics but GNSS-measured velocity of a few mm/yr. This case may indicate underestimation due to LOS measurements, but also highlight the difference between the point-based locations of the GNSS data and the InSAR averaged values over 40 m pixels. For the other case, the difference is inversed (no significative GNSS movement but mm–cm/yr InSAR-based kinematics), which may also indicate that the locations of the GNSS measurements are not necessarily representative of the whole mass. Overall, 15 out of 17 comparable rockslides are correctly categorized, which is considered as a good proportion considering the differences of measurement properties and low velocities of these objects (point-scale vs 40 m pixels, 2–3D vs 1D LOS).

Feature tracking on repeat optical airphotos [RD-34] for two rock glaciers in Signaldalen and one at Skaiddevarri (CCI-07-0316, CCI-07-0330, CCI-07-0172) has been performed to derive 2011-2016 average velocities [RD-34]. Their average speeds were 1.0, 0.65, and 0.75 m/yr, e.g. mostly between 1-2 m/yr for CCI-07-0316 and 0.5-1 m/yr for CCI-07-0330 & CCI-07-0172. The results are in agreement with the order of magnitude documented by the InSAR-based kinematic attributes in RGI (m/yr for CCI-07-0316; dm-m/yr for CCI-07-0330 and CCI-07-0172). The detailed velocity fields available from our photogrammetric measurements show spatio-temporal variations that underline that the boundaries between RGI velocity classes are a reliable quantitative indicator but should not be treated absolutely sharp as they may have small uncertainties depending on which exact rock glacier section they refer to.
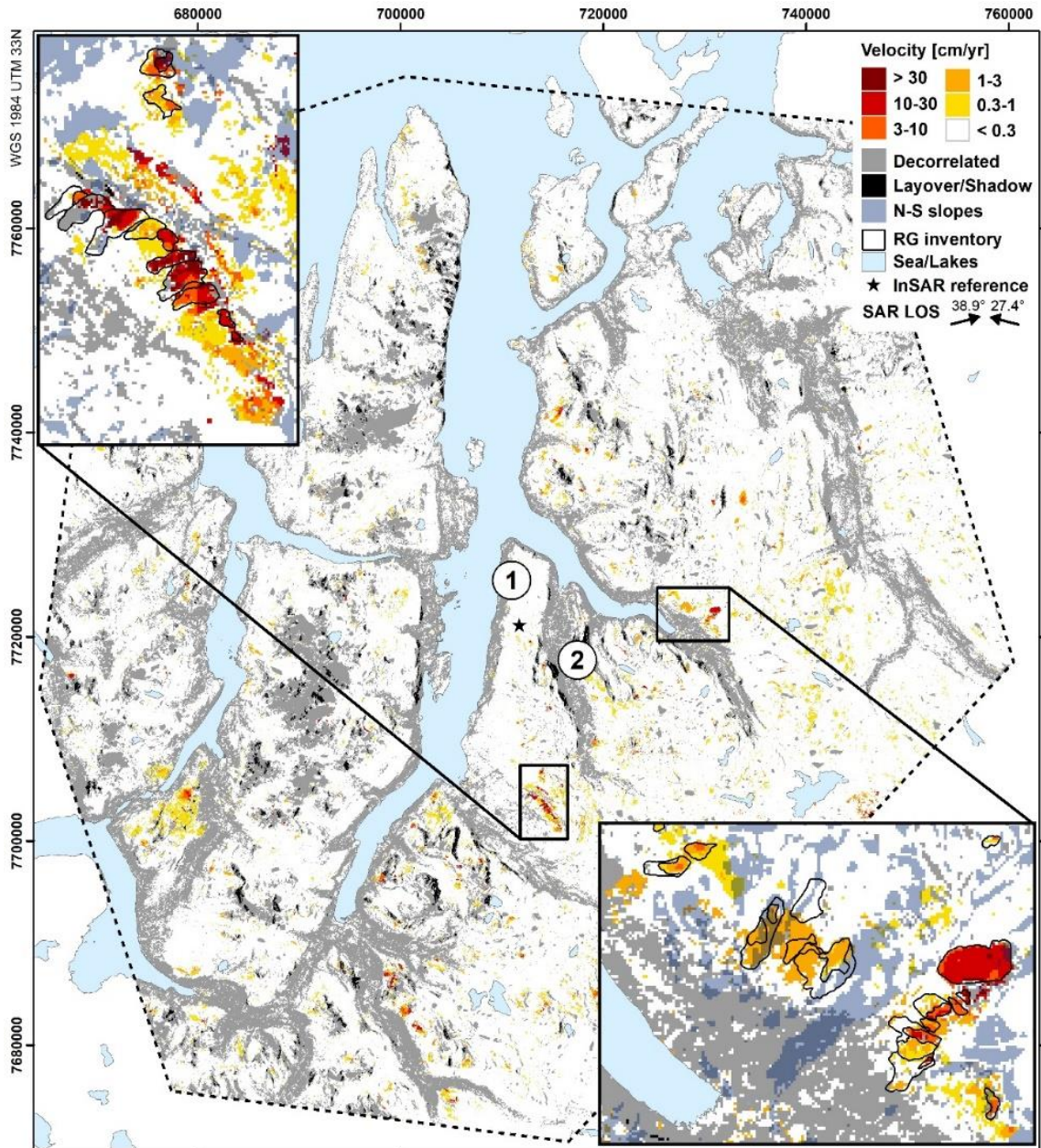
Figure 2.3.2.1: InSAR moving areas (MA) over Troms study area and detailed views over Ádjet (Skibotndalen, upper-left inset) and Njárgavárri/Badjánvárri (Kåfjorddalen, lower-right inset). Numbers 1–2 are the locations of areas detailed in Figure 2.3.2.2.
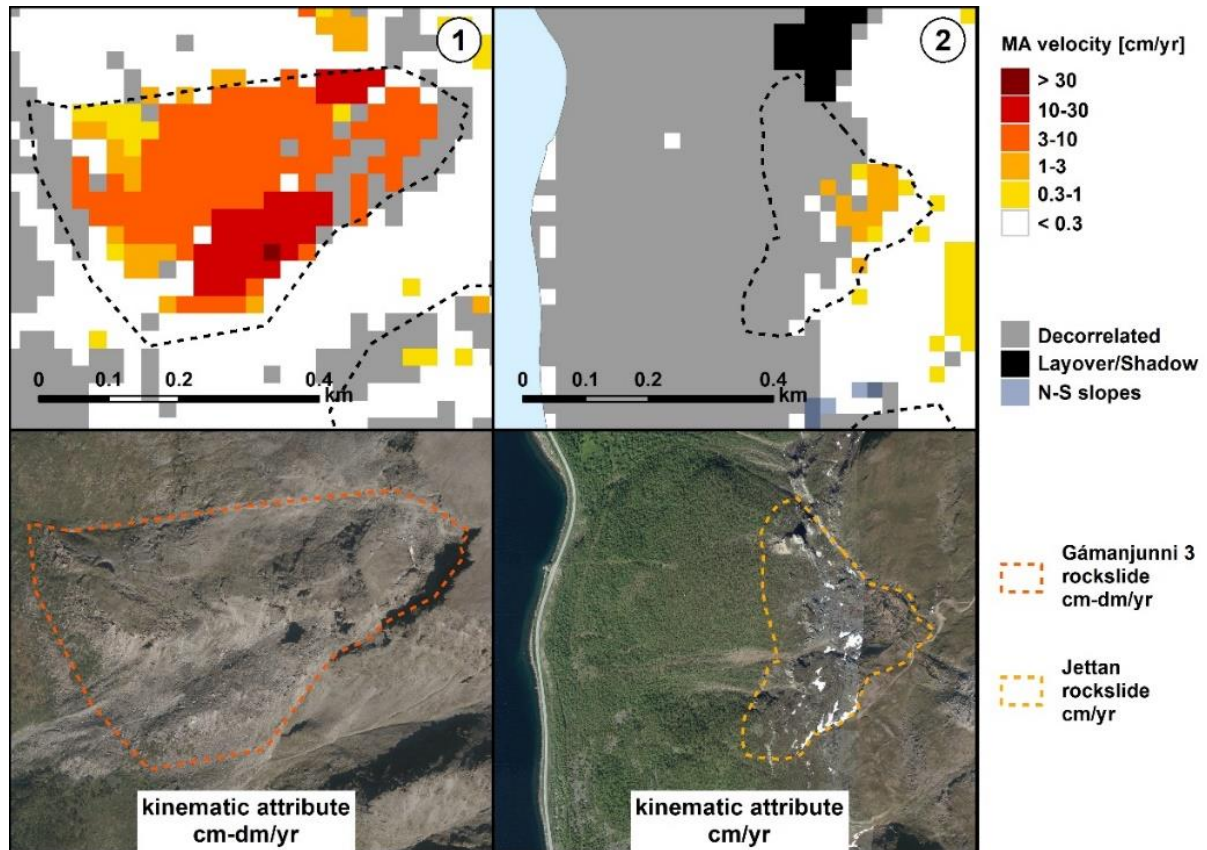
Figure 2.3.2.2: Detailed maps over two high-risk rockslides of Troms study area: 1) Gámánjuuni 3 and 2) Jettan. Both landforms are continuously monitored. In-situ measurements from the Norwegian Water Resources and Energy directorate (NVE) and the Geological Survey of Norway (NGU) show velocity ranges in the similar order of magnitude as the assigned kinematic attribute, based on the InSAR moving areas (MA).

In Finnmark, Hopefjorden is the area with the highest density of inventoried landforms (Figure 2.3.2.3) and is characterized by little activity, with no or slow movement in lower slopes of the main rock systems and higher detected velocity in the upper slopes. InSAR kinematics show that most of the inventoried landforms are relict or transitional, which fits with expert assessment (Karianne Lilleøren and Bernd Etzelmüller, UiO). At the head of Ivarsfjorden, complementary measurements based on aerial imagery (drone and manned aircraft) highlighted velocity in mm/yr to cm/yr ranges with localized areas up to 10 cm/yr, which overall fit well with InSAR moving areas. The results are overall consistent with InSAR Norway, although some localized areas classified InSAR stacking results seems to be affected by atmospheric/ionospheric effects.
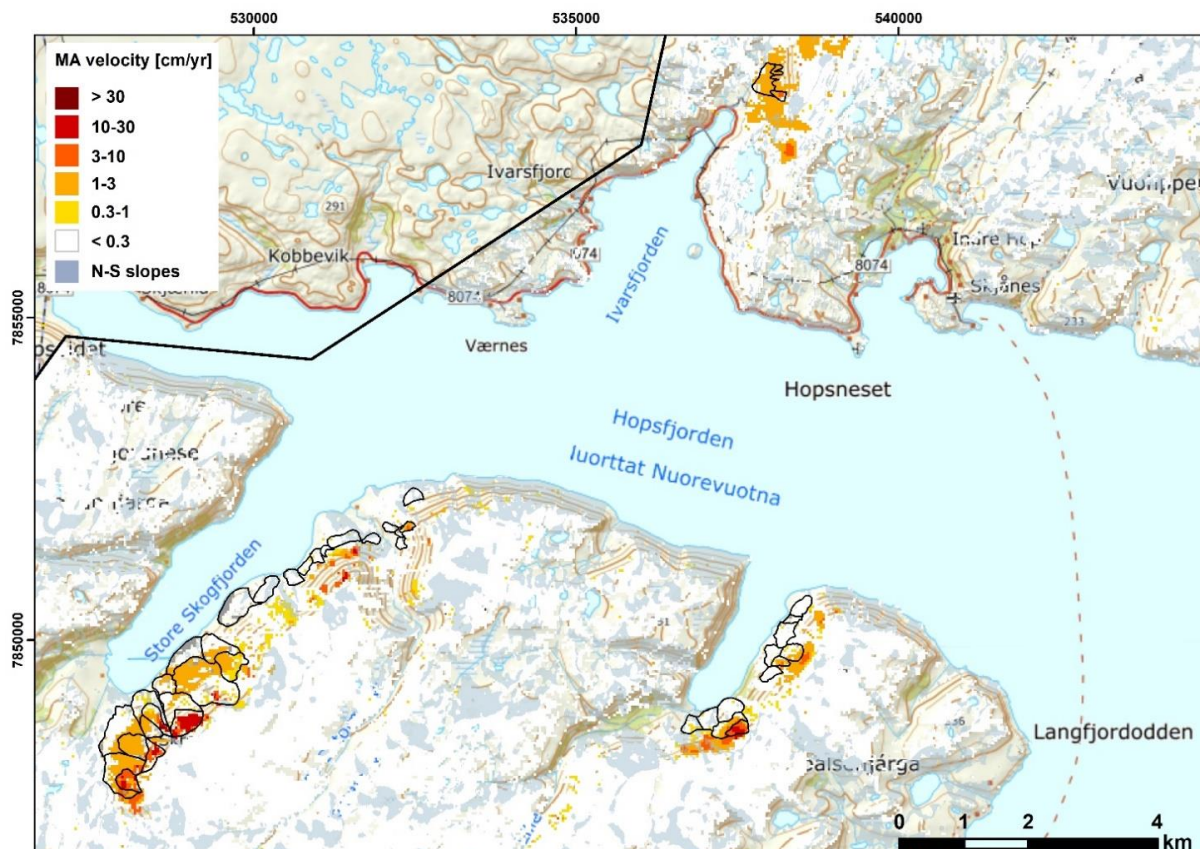
Figure 2.3.2.3: InSAR moving areas (MA) in a selected part of the Finnmark area which is well studied by UiO. Black lines: indicative delineations of the inventoried rock glaciers.

In Svalbard, the whole landscape is highly dynamic. Although many processes are seasonal and cyclic, the rates are expressed as annual averages due to the focus on rock glacier creep. In flat areas, seasonal settlement varies depending on the ice content in the active layer: little movement over built surface in Longyearbyen and close to the airport (Figure 2.3.2.4) and large movement in ice-rich valley bottoms (e.g. Adventdalen, Figure 2.3.2.4). This distribution fits to the expectation from expert assessment (Hanne H. Christiansen, UNIS; Ole Humlum, ArcticHero). The 'Huset' rock glacier in Longyearbyen is monitored by annual GPS and inclinometer measurements (collaboration between the University of Tsukuba and UNIS). Creep rates documented since 2009 are between 2.4 and 5 cm/yr (Matsuoka et al., 2019). The InSAR moving areas highlight similar velocities (1–3 and 3–10 cm/yr within NE blue delineation, Figure 2.3.2.4). The rock glacier kinematic attribute based on InSAR has been set to cm–dm/yr. The neighbouring 'Sverdrupbyen' rock glacier (SW blue delineation, Figure 2.3.2.4) has a higher creep rate (dm/yr), that has also been previously documented by complementary InSAR studies based on other sensors and methods (Rouyet et al., 2017; 2019). In Endalen, two-dimensional (vertical and along slope) movement is continuously measured by a solifluction station (Harris et al., 2011) (blue dot, Figure 2.3.2.4). Documented measurements show cm–dm/yr seasonal thaw settlement and cm/yr net surface downslope movement at this location (Harris et al., 2011). InSAR moving areas in this area are between 1–3 and 3–10 cm/yr, which is consistent with the in-situ data.

For a large rock glacier complex at Nordenskiöldkysten (upper left zoom panel in [RD-34], Fig. 2.2.6.1) the InSAR-derived RGI kinematic class indicates mm-cm/yr. This is consistent with aerophotogrammetric measurements over 1970-1990 that did not find any significant movement, e.g.

movement <= 1 cm/yr (Kääb et al., 2002). The latter study also found movement of several cm/yr in a small section of the upper talus, also in agreement with the InSAR results used for RGI kinematic classification (Fig. 2.2.6.1 in [RD-34]).
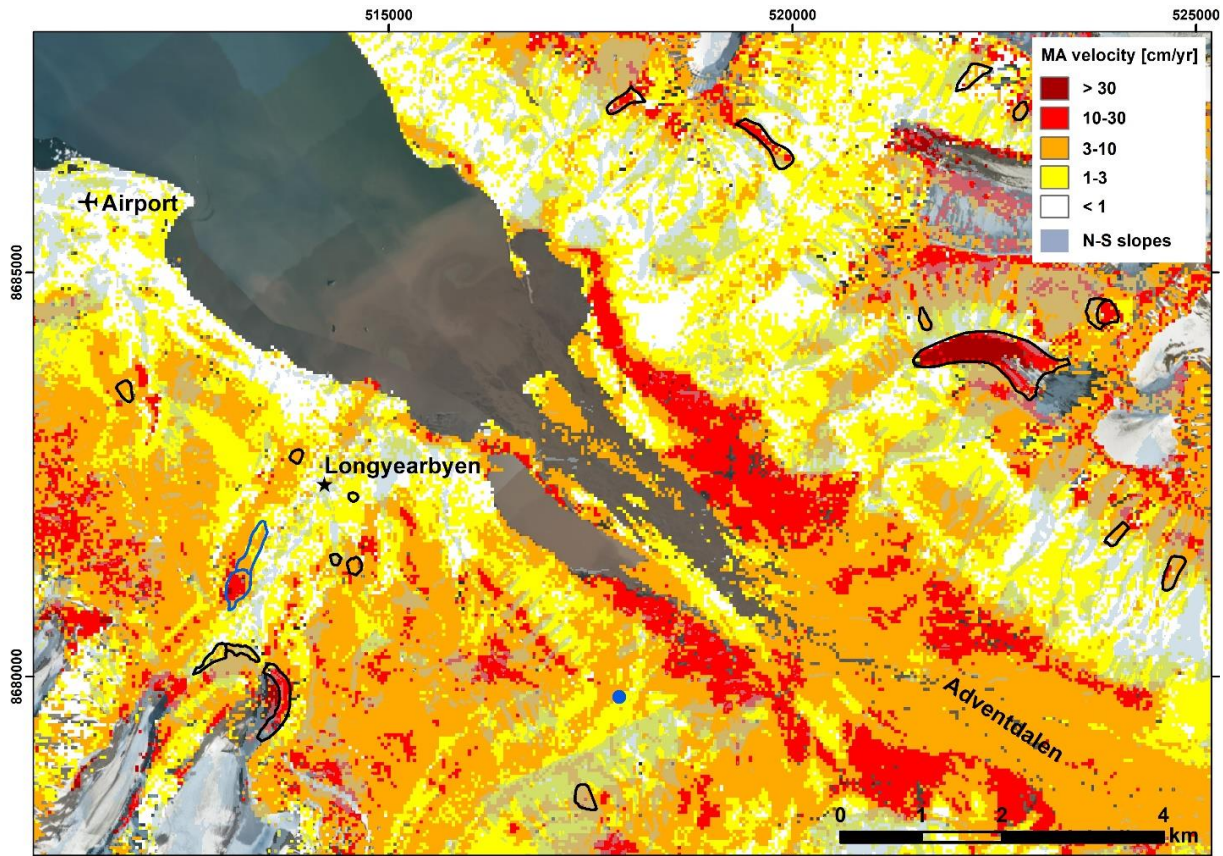

Figure 2.3.2.4: InSAR moving areas (MA) in a selected part of Svalbard study area (Longyeardalen, Adventdalen, Endalen) well studied by UNIS. Blue dot: Endalen solifluction station. Blue rock glaciers (indicative delineations): Huset and Sverdrupbyen rock glaciers. Black lines: other inventoried rock glaciers (indicative delineations).

2.3.3 Validation for Vanoise Massif (France) study area

On the complex of active rock glaciers Lou, repeated GNSS annual survey of blocks during the 2018-2019 period yields surface velocities ranging from several meters per year on the fastest Western lobe to 50-100 cm per year on the Eastern lobe. Taking into account that the movement of the RG complex is mostly South-North, two moving areas were mapped, one over most of the landform with a velocity class of 10-30 cm/yr, and a smaller one on the Western lobe with a > 100 cm/yr class. The rock glacier complex was classified as "m/yr".

2.3.4 Validation for Central Andes (Argentina) study area

Trombotto-Liaudat and Bottegal (2019) collected independent measurements of surface displacement for Morenas Coloradas rock glacier (ID CCI-15-08036-00) for the austral summer and winter of 2013, 2014, and 2015. Using repeated GNSS measurement of GCPs located on individual boulders in the rock glacier's lower reach, they found horizontal displacements in the range of 40 cm/yr to 300 cm/yr

with some seasonal variations. More recently, Blöthe and others (2020) collected independent measurements of the surface displacement of Morenas Coloradas (ID CCI-15-08036-00) and Stepanek (ID CCI-15-08440-00) rock glaciers for the austral summers of 2017, 2018, and 2019. Using repeated GNSS measurement of GCPs located on individual boulders in the rock glaciers' lower reach, they found horizontal displacements of >3.0 m/yr (range of 0.5 to 3.5 m/yr) and >1.5 m/yr, for Morenas Coloradas and Stepanek, respectively. Morenas Coloradas moving areas were mapped with InSAR data with a velocity class of >100 cm/yr. Meanwhile, Stepanek's moving area was mapped with velocity class 30-100 cm/yr. For both rock glaciers, the spatial pattern of surface displacement interpreted from the Sentinel-1 single interferograms and the 6 or 12 days stacking maps agrees with the spatial pattern observed in the GNSS measurements.

2.3.5 Validation for Southern Alps (New Zealand) study area

The kinematics of two rock glaciers located in the Irishman stream, Ben Ohau range, was investigated through two GNSS measurements campaigns in January 2016 and February 2017. Rock glacier I has horizontal surface velocities lower than 3 cm/yr. With InSAR data a moving area with velocities lower than 1 cm/yr was detected. Velocities measured on rock glacier II are comprised between 2-5 cm/yr in the lower part and up to 14 cm near the roots. An InSAR-detected moving area of 3-10 cm/ry was mapped for this rock glacier. For rock glacier I the InSAR velocity is therefore slight underestimated, while for the rock glacier II the spatial pattern of surface displacement interpreted from InSAR agrees with the spatial pattern observed in the GNSS measurements.

2.3.6 Validation for the Tien Shan study area

For six rock glaciers of an InSAR-derived rock glacier kinematic inventory in Ile Alatau and Kungöy Ala-Too, northern Tien Shan, Kääb et al. (2021) compared the inventory results to offset tracking based on repeat high-resolution optical satellite data. For all six rock glaciers the velocity class was correctly determined. The photogrammetric velocity fields enable also a more detailed comparison of the delineations of moving areas (Fig. 2.3.6.1). Overall, the InSAR outlines fit very well to the photogrammetric velocity fields. The only notable problem identified is that areas with interferometric phase decorrelation within or at the margins of rock glaciers might be classified as > 1m/yr class, assuming motion decorrelation, while in reality the decorrelation might be induced by thermokarst processes, e.g. by temporal decorrelation destroying the surface. Figure 2.3.6.1 shows one comparison between an interferogram and photogrammetric velocities, the other comparisons are found in the Supplement of Kääb et al. (2021).
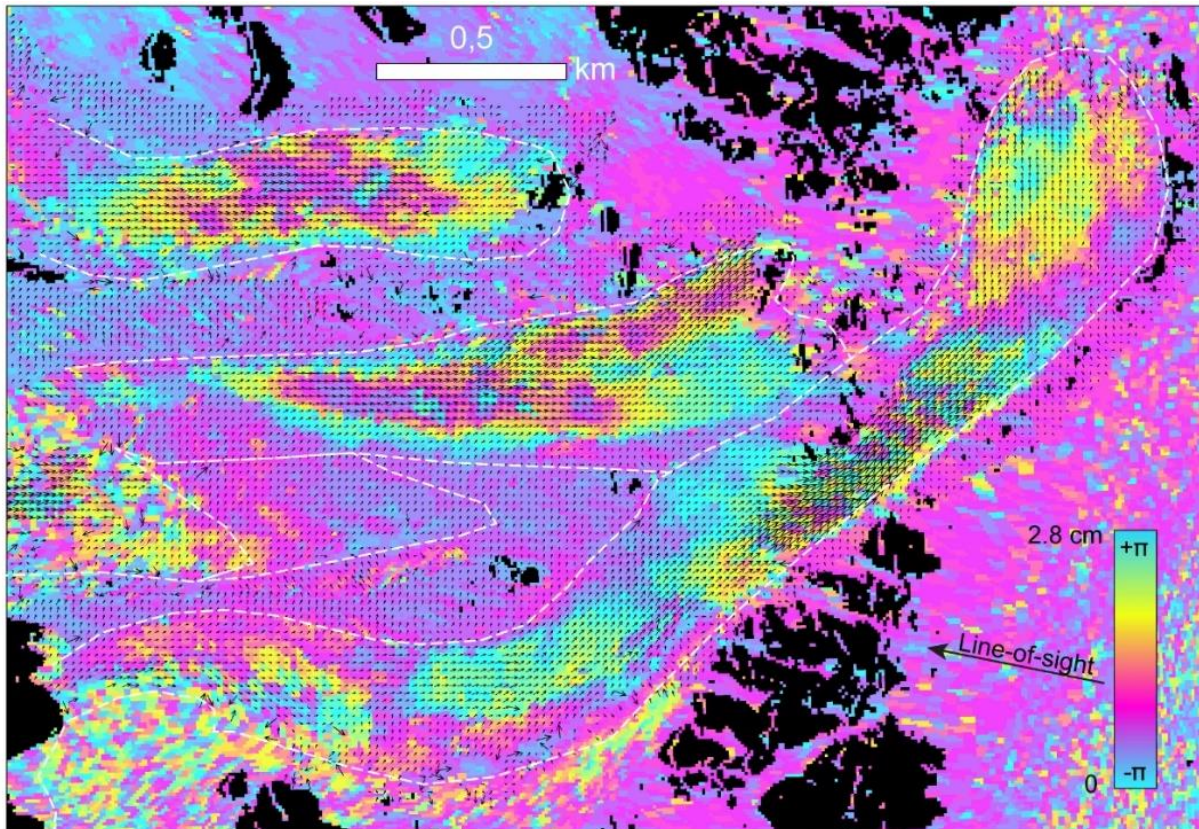
Figure 2.3.6.1: Ordzhonikidze rock glacier, Tien Shan. Section of a interferogram between Sentinel-1 radar data of 24 Aug and 5 Sep 2018 (12 days) with vectors superimposed from image matching between 2016 and 2018 high resolution satellite images. The white dashed lines are the inventory outline polygons from motion and process-type classes. Photogrammetric velocities are up to 4 m/yr. Similar comparisons for the other rock glaciers are displayed in the Supplement of Kääb et al. (2021).

2.3.7 Validation for the Brooks Range study area

Since 2012, a research team has made independent measurements of surface movement of eight frozen debris lobes (FDLs) in the Alaskan Brooks Range. Measurements are made using a real-time kinematic global positioning system (RTK-GPS). Six of these FDLs are included in the current rock glacier study area (table 2.3.7.1). The RTK-GPS rates reported are the annualized average rate of all surface measurements across the FDL. With the exception of FDL-A, rates are typically measured only once a year.

FDL (*FID#*)	INSAR ANALYSIS (USING PALSAR2)		GNSS	
	PERIOD OF COVERAGE	VELOCITY DETERMINATION	PERIOD OF COVERAGE	RTK-GPS AVG. RATE (M/YR)
FDL-11 (*FID270*)	2015-2016	INCOHERENT	201508-201608	0.17
FDL-7 (*FID37*)	20160613_20160627	>300 CM/YR, VELOCITY CLASS 6	201508-201608	13.0
FDL-B (*FID33*)	20150314_20150328	VARIABLE MOTION, VELOCITY CLASS 6	201408-201508	2.1
FDL-A (*FID32*)	20150527_20150610	>300 CM/YR, VELOCITY CLASS 6	20150521_20150821	5.7
FDL-C (*FID31*)	20150527_20150610	>300 CM/YR, VELOCITY CLASS 6	201408-201508	0.9
FDL-D (*FID57*)	20150314_20150328	DECORRELATED	201408-201508	15.0

Table 2.3.7.1: Comparison between InSAR and GNSS measurements on six Frozen debris lobes (FLD) in the Brooks range.

2.4. Results consolidation

2.4.1 Consolidation for Swiss Alps study area

The consolidation phase with the second operator did not highlight any major discrepancies. The main differences were found in the assignment of the velocity classes of the moving areas, especially when there was a great variability of velocity (in time and space). Differences were also found on the assignment of the degree of reliability both for the moving areas and for the rock glaciers, as it is more subjective.

Finally, discrepancies were detected in the identification of rock glacier units (e.g. underestimation or overestimation of the number of rock glacier units). However, the definition of a rock glacier unit is still being developed by the IPA Action Group and specific guidelines are not yet ready.

2.4.2 Consolidation for Norwegian study areas

A complete consolidation phase with a second operator has not been performed yet for the Norwegian study areas. The same person was the main operator for the three areas, which has the advantage of consistency but the drawback of a potential systematic subjectivity. A phase of verification and corrections with contributions of experts in geomorphology has however been performed for the three areas: in Troms and Finnmark with contributions from Karianne S. Lilleøren, Bernd Etzelmüller and Reynald Delaloye, in Svalbard with the contributions from Hanne H. Christiansen and Ole Humlum. This phase led to several modifications: removal of misclassified landforms, change of attributes, adjustments of delineations and unit's division, better interpretation of kinematics for specific landforms.

3 Rock Glacier Kinematic Time Series

3.1 Kinematic time series from InSAR measurements

3.1.1. Methods for quality assessment

As described in the End-to-End ECV Uncertainty Budget (E3UB) [RD-26], there are various approaches to estimate the uncertainty of InSAR measurements, including a formal description of the error terms, internal quality measures, analysis of interferometric phase on stable ground, comparison against results from other satellite data, and/or ground-based measurements (e.g. from GNSS).

3.1.2 Reference data

One of the permanent mono-frequency GNSS stations over Becs-de-Bosson rock glacier (Switzerland), which was installed in 2016 at a location where velocities are rather spatially homogeneous, was used for a direct validation of the Sentinel-1 InSAR measurements (Strozzi et al., 2020). In local differential mode, with postprocessing computed with respect to a permanent local basis, the estimated accuracy of the mean planimetric and altimetric GNSS positioning over 24 hours is in the order of +/-2 mm and that of the velocity over a 6 day period in the order of +/-0.24 m/yr (Wirz et al., 2014).

Over the Distelhorn rock glacier (Switzerland), orthorectified aerial images provided by Swisstopo, the Swiss national mapping agency, with a spatial resolution of 0.4 m acquired on 03.09.2014 and 21.09.2017 were matched with standard normalized image cross-correlation techniques (Strozzi et al., 2020). From matches over stable ground outside the rock glacier a displacement accuracy of ±0.15 m, that is, ±0.05 m/yr, was estimated.

3.1.3 Match up analyses

A formal description of error terms [RD-26] for single measurements at C-band indicates a LOS measurement uncertainty of ±0.4 m/yr for Sentinel-1 interferograms over six days and of ±0.2 m/yr for Sentinel-1 interferograms over 12 days and can go down to a mm-accuracy using multi-temporal techniques.

The 3D GNSS velocities computed with the average daily positions corresponding to the acquisition dates of the Sentinel-1 images over Becs-de-Bosson rock glacier (Switzerland) are plotted together with the velocities along the maximum slope direction from Sentinel-1 InSAR in Figure 3.1.3.1. For the 41 coincident measurement points, the standard deviation of the velocity difference is 0.21 m/yr, while average, minimum, and maximum of the velocity difference are -0.08 m/yr, -0.67 m/yr, and 0.33 m/yr, respectively. Sentinel-1 InSAR is slightly underestimating the velocities at GNSS locations, possibly because the rock glacier is not exactly moving along the steepest slope or as a result of the InSAR spatial resolution on the order of 15 m.
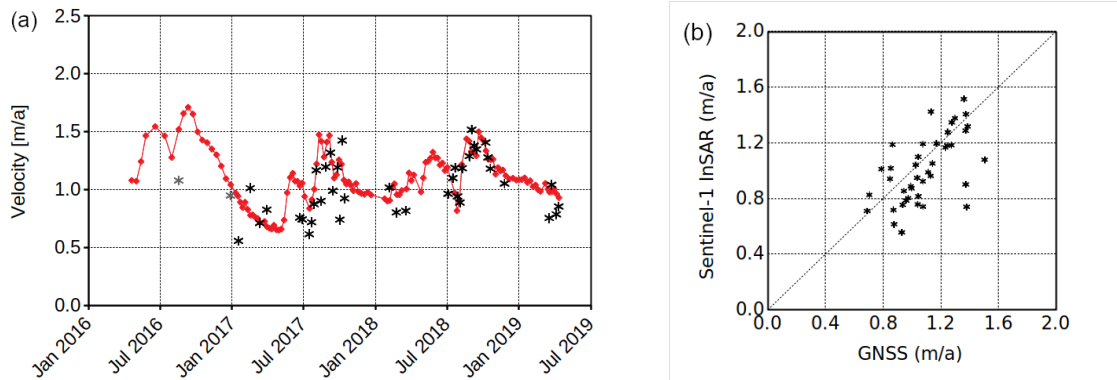
Figure 3.1.3.1: Three-dimensional (3D) GNSS velocities computed with the average daily positions corresponding to the acquisition dates of the Sentinel-1 acquisitions (red diamonds) and velocity along the maximum slope direction from Sentinel-1 InSAR (grey 12 day time interval, black 6 day time interval) at GNSS station BdB2 over Becs-de-Besson rock glacier (Val de Réchy, Switzerland); (b) Scatter plot of GNSS and Sentinel-1 InSAR velocities at 41 measurements points (Strozzi et al., 2020).

The horizontal displacement field from matching orthorectified aerial images over Distelhorn rock glacier (Switzerland) on 03.09.2014 and 21.09.2017 is compared to the Sentinel-1 InSAR LOS displacement field from 02.08.2018 to 08.08.2018 in Figure 3.1.3.2 along with the difference map between the two measurements. The results of Figure 3.1.3.2 indicate a good spatial correspondence between aerial photo matching and Sentinel-1 InSAR, but on the southern tip of the rock glacier the interferogram was not correctly unwrapped. Further discrepancies can be observed on the edges of the fastest moving parts of the rock glacier front. The scatter plot of the aerial photo matching and Sentinel-1 LOS velocities (Figure 3.1.3.3) indicates the effect of the different time intervals (three years as compared with six days) and of the satellite look direction. In Figure 3.1.3.2 b, we empirically fitted the Sentinel-1 LOS velocities to the aerial photo matching velocities by scaling them with a factor of -1.23 in order to maximize the one-to-one match and to account for these two effects. After scaling, the standard deviation of the velocity difference for the 2237 coincident measurement points is 0.30 m/yr, while average, minimum and maximum velocity differences are 0.01 m/yr, -2.09 m/yr, and 2.84 m/yr, respectively. After removal of the 17 wrongly unwrapped Sentinel-1 InSAR points in the southern tip of the rock glacier, the standard deviation of the velocity difference is 0.25 m/yr, while average, minimum, and maximum velocity differences are 0.00 m/yr, -1.28 m/yr, and 1.50 m/yr, respectively.
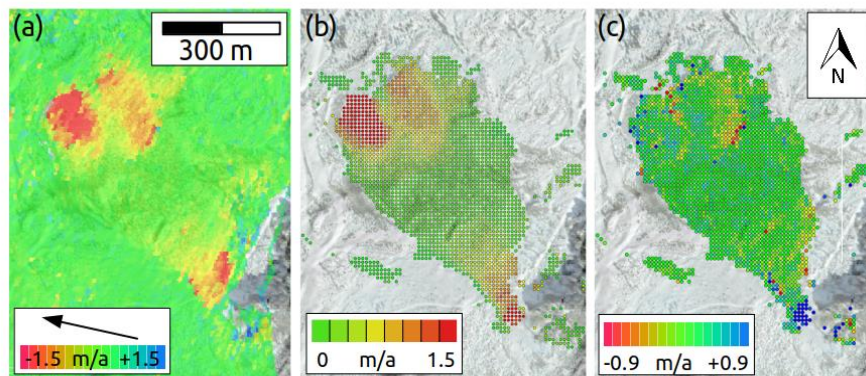
Figure 3.1.3.2: Distelhorn rock glacier (Mattertal, Switzerland). (a) Sentinel-1 InSAR line-of-sight velocity map from 02.08.2018 to 08.08.2018; (b) Horizontal velocity map from matching of aerial optical images with a spatial resolution of 0.15 m acquired on 03.09.2014 and 21.09.2017; (c) Difference map between aerial photo matching and Sentinel-1 InSAR LOS velocities (Reference Strozzi et al., 2020).
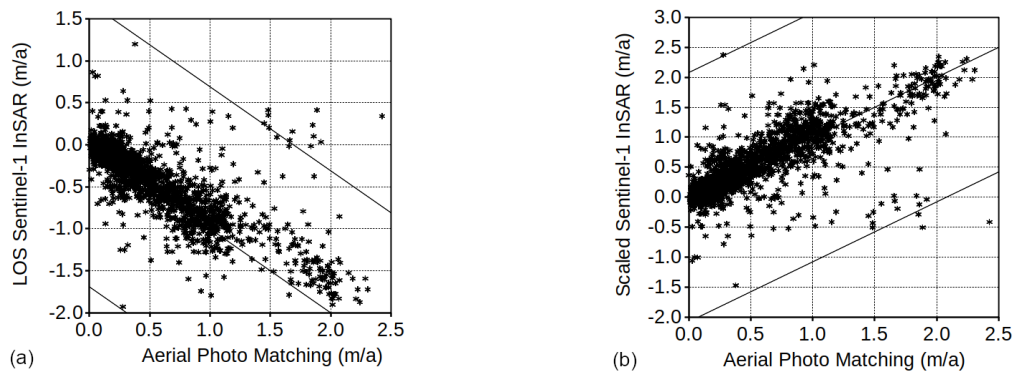

Figure 3.1.3.3: Distelhorn rock glacier (Mattertal, Switzerland). (a) Scatter plot of the horizontal velocities from matching of aerial optical images between 03.09.2014 and 21.09.2017 and of Sentinel-1 InSAR line-of-sight velocities from 02.08.2018 to 08.08.2018; (b) Scatter plot of the aerial photo matching and scaled (factor -1.23) Sentinel-1 InSAR velocities. The lines indicate the 1:1 matching and the -2p and +2p ambiguities (Reference Strozzi et al., 2020).

3.1.4 Discussion

With Sentinel-1, satellite SAR images that enable interferometry are nowadays regularly acquired worldwide. Therefore, this mission provides consistent time series of rock glacier velocities every six days over Europe and Greenland and every 12 days over other mountainous regions, including the Andes of South America. The estimated accuracy of the Sentinel-1 InSAR measurements is in the order of 0.2 m/yr. Typical lower and upper limits of detection for six days data are in the order of 0.4 m/yr (e.g. , 6 mm/6 days or 1 mm/day) and 2 m/yr (e.g. , 2.8 cm/6 days or 0.5 cm/day), respectively. Monitoring the kinematics of rock glaciers with Sentinel-1 SAR interferometry is, however, limited by the spatial resolution of the SAR data of about 15 m on the ground for a multi-looking factor of 4 pixels in range and 1 pixel in azimuth. It is, therefore, essential to select a representative point over the rock glacier, where the spatial variability of the motion around is low, in order to extract a meaningful

time series of motion. In addition, Sentinel-1, as all other SAR missions, suffers in rugged terrain from incomplete spatial coverage due to layover/shadow and sensitivity to motion restricted to the LOS. For our analyses, we projected, therefore, the InSAR LOS motion along the maximum slope direction.

3.2 Kinematic time series from SAR offset tracking

3.2.1. Methods for quality assessment

As described in the End-to-End ECV Uncertainty Budget (E3UB) [RD-26], there are various approaches to estimate the uncertainty of SAR offset-tracking measurements, including internal quality measures, matching on stable ground, comparison against results from other satellite data, and/or ground-based measurements (e.g. from GNSS).

3.2.2 Reference data

Over the Distelhorn rock glacier (Switzerland), orthorectified aerial images provided by Swisstopo, the Swiss national mapping agency, with a spatial resolution of 0.4 m acquired on 03.09.2014 and 21.09.2017 were matched with standard normalized image cross-correlation techniques (Strozzi et al., 2020). From matches over stable ground outside the rock glacier a displacement accuracy of ±0.15 m, that is, ±0.05 m/yr, was estimated.

3.2.3 Match up analyses

Paul at al. (2017) investigated the accuracy of SAR offset tracking for ice surface velocity estimation in various aspects, including a formal description of the error terms, matching on stable ground, comparison against results from SAR image data of equal or better resolution, and ground-based measurements from GNSS. They estimated the reliability of the cross-correlation algorithm to return coregistration parameters in the order of 1/10th of a SAR image pixel. This corresponds for the TerraSAR-X to an accuracy of about 0.3 m in measuring horizontal displacement (measured along the range and azimuth directions of the satellite).

Offset tracking based on TerraSAR-X images over the Distelhorn rock glacier was performed with time intervals of about two years. Therefore, a coregistration precision of 1/10th of a SAR image pixel would correspond to 0.15 m/yr in measuring horizontal displacement. Statistical measures of displacement were computed for every TerraSAR-X image pair over 55,580 points on stable terrain surrounding the rock glacier. The mean of the horizontal velocities for the four image pairs 24.09.2008 to 20.09.2010, 09.09.2010 to 04.09.2012, 15.09.2012 to 22.09.2014, and 11.09.2014 to 06.09.2016 were 0.42 m, 0.43 m, 0.42 m, and 0.48 m, respectively, on average 0.22 m/yr. The standard deviations of the estimates for the four image pairs were 0.45 m, 0.54 m, 0.44 m, and 0.46 m, respectively, on average 0.24 m/yr.

A visual comparison to the matching of aerial optical images acquired on 03.09.2014 and 21.09.2017 was drawn, as shown in Figure 3.2.1.1. These results clearly point to the lower spatial resolution of

TerraSAR-X offset tracking with respect to matching of aerial optical images, with large discrepancies on the edges of the fastest moving parts of the rock glacier. The scatter plot of the aerial photo matching and TerraSAR-X velocities (Figure 3.2.1.2) also indicates a bias of the offset tracking results, which are generally lower than those from the matching of aerial images as a result of the larger cross-correlation window size used with SAR images. The standard deviation of the velocity difference for the 2,197 coincident measurement points is 0.34 m/yr, while average, minimum, and maximum velocity differences are -0.22 m/yr, -2.61 m/yr, and 1.87 m/yr, respectively. With very high-resolution X-band SAR data, employed over rock glaciers using SAR offset tracking, the estimated accuracy is in the order of 0.3 m/yr for a time interval of two years. Displacements of more than 3 m/yr could be successfully detected with SAR offset tracking, but the spatial resolution is poor (~125 m), and therefore detailed spatial variabilities of motion cannot be captured.
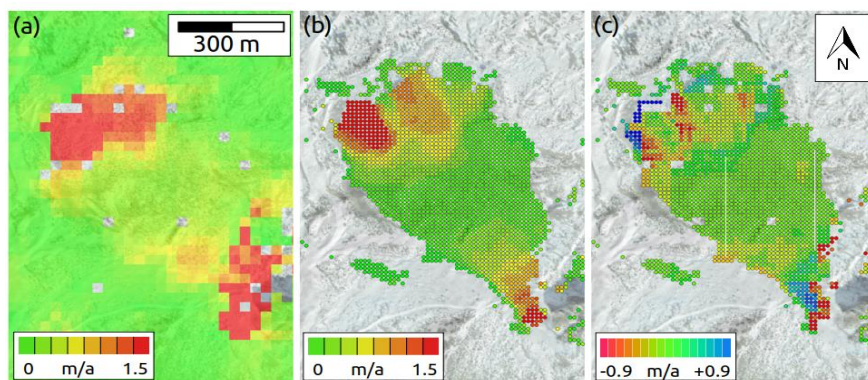

Figure 3.2.1.1: Distelhorn rock glacier (Mattertal, Switzerland). (a) Horizontal velocity map from TerraSAR-X offset tracking between 11.09.2014 and 06.09.2016; (b) Horizontal velocity map from matching of aerial optical images with a spatial resolution of 0.15 m acquired on 03.09.2014 and 21.09.2017; (c) Difference map between aerial photo matching and TerraSAR-X offset tracking velocities (Strozzi et al., 2020).
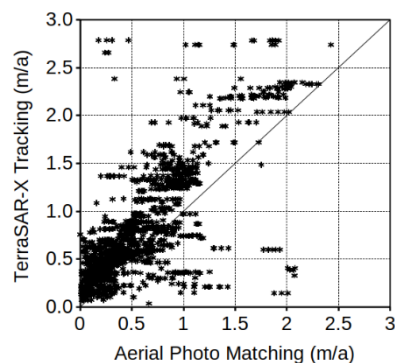

Figure 3.2.1.2: Distelhorn rock glacier (Mattertal, Switzerland). Scatter plot of the horizontal velocities from matching of aerial optical images between 03.09.2014 and 21.09.2017 and TerraSAR-X offset tracking between 11.09.2014 and 06.09.2016 (Strozzi et al., 2020).

3.2.4 Discussion

The offset tracking and InSAR are highly complementary techniques in terms of detection capability. For high velocity, offset tracking is more suitable since the InSAR technique is limited by the

wavelength of the satellite, while for low velocity, the SAR offset tracking is not suitable because of the low displacement sensitivity.

3.3 Kinematic time series from optical data

3.3.1. Methods for quality assessment

As described in the End-to-End ECV Uncertainty Budget (E3UB) [RD-26], there are various approaches to estimate the uncertainty of optical offset-tracking measurements, including internal quality measures, matching on stable ground, comparison against results from other satellite data, and/or ground-based measurements (e.g. from GNSS).

3.3.2 Reference data

The InSAR and SAR offset tracking measurements of sections 3.1 and 3.2 become in the case of optical tracking the reference data, while the optical tracking data served as reference data in sections 3.1 (3.1.2) and 3.2 (3.2.2)

3.3.3 Match up analyses

Match-up analyses between InSAR and SAR offset tracking results are shown and discussed in sections 3.1.3 and 3.2.3/4. In general, InSAR and optical tracking are complementary rather than exchangeable due to their different sensitivity to the magnitude of velocity (see 3.2.4). As such, direct comparisons are always under an assumption of temporal changes, for instance assuming a scaling factor (3.1.3). The very different temporal resolutions of optical tracking (years) and InSAR (weeks) prohibits strict direct match-ups.

3.4 Trends in rock glaciers velocity in Southern Carpathians (Romania)

3.4.1 Methods for quality assessment

In the presence of ground-based levelling or GNSS measurements with deterministic measurement errors that should be in the same range as InSAR or better, the **absolute** quality measure of the InSAR measurements would result from correlation with the ground-based measurements.

In the absence of ground-based measurements (with known, deterministic errors), the **relative** quality measure for the InSAR measurements could be estimated from matching up in a least square sense based on displacement rates extracted from independent measurements (interferograms acquired at different dates that contain temporal redundancy).

A **visual** assessment of the results is represented by direct comparison between the detected areas with measured dynamics and the permafrost distribution model. Also, the comparison of displacement fields generated from independent data sets from different sensors covering the same period can be used for uncertainty estimation. It has, however, to be considered that often the temporal and spatial representativeness of the data is not assured, introducing additional constraints on the validation.

3.4.2 Reference Data

Due to a lack of continuous long-term data on rock glaciers kinematics in Romania, we started to survey two rock glaciers in the Retezat Mountains by repeated differential GNSS measurements within CCN1. A TopCon Hiper V Differential GPS was used to acquire high precision positioning data. The Hiper V receiver is built with a high-performance 3.5 G modem and a UHF radio card that allows the receiver to be connected to the reference networks (e.g. ROMPOS – Romanian real-time positioning network) but also to be used in a Base-Rover (RTK) configuration. Within the area of the Judele and Peleaga rock glaciers (Retezat Mountains) the points were collected using a classic Base-Rover configuration (Figure 3.4.1). The first base point was created on Bucura Ridge where the ROMPOS network was used for real-time corrections in order to measure a point with very high precision. Therefore, each point on the glaciers was measured with millimetric precision. Following this approach, 26 points have been surveyed at several key locations over the rock glaciers. Measuring these points with millimeter accuracy enables us to determine displacements, if any, through successive seasonal data acquisitions. Two successive measurement campaigns (12 August and 14 October) were carried out in 2019. Due to the short time between the measurements, no rock displacement was observed. In order to obtain meaningful results using this methodology, these measurements should be carried out over several consecutive years.

A multiannual velocity measurement has been performed between 2012 and 2014 in the Retezat Mountains using a geodetic survey method (Popescu, 2015b). The resulting velocity map is considered as an independent result for visual assessment of the velocity maps produced by the current project.

Existing geophysical measurements (electrical resistivity tomography and ground penetrating radar) reveal the patchy distribution of permafrost within four rock glaciers in the Retezat Mountains and are also used to confirm that the ground displacement is due to permafrost creep and not due to other processes (e.g., solifluction, frost heaving, rockfalls etc.). Existing ground surface temperature data on six rock glaciers in the Retezat Mountains will serve as basis for the assessment of the relation between local climatic conditions and rock glacier kinematics. ERT profiles were performed for three rock glaciers in the Retezat Mountains. They revealed high resistivity values, which likely represent ice-rich frozen debris (Figure 3.4.2). These high resistivity values, reaching 100 kΩm, were found at 5-10 m depth below the surface in all the cases (Onaca et al., 2015).

The first rock glacier inventory in the highest mountains of the Romanian Carpathians was compiled by Urdea (1998). This incomplete inventory consisted of analogue drawings of rock glaciers contours on topographic maps at scale 1:25 000 for several mountain ranges (Retezat, Făgăraș and the western part of Parâng Mountains). More recently, using high quality air-orthophoto data and high-resolution

topography data and a complementary field work survey, Onaca et al. (2017), realized the first polygon-based inventory of rock glaciers for the Southern Carpathians.

A series of ALOS-2 PALSAR-2 data of the ascending orbit is also available over the two areas of interest. We considered images acquired during the snow-free period between 2014 and 2019. These data were provided by JAXA and are courtesy of RA6-3016 (P.I. T. Strozzi).
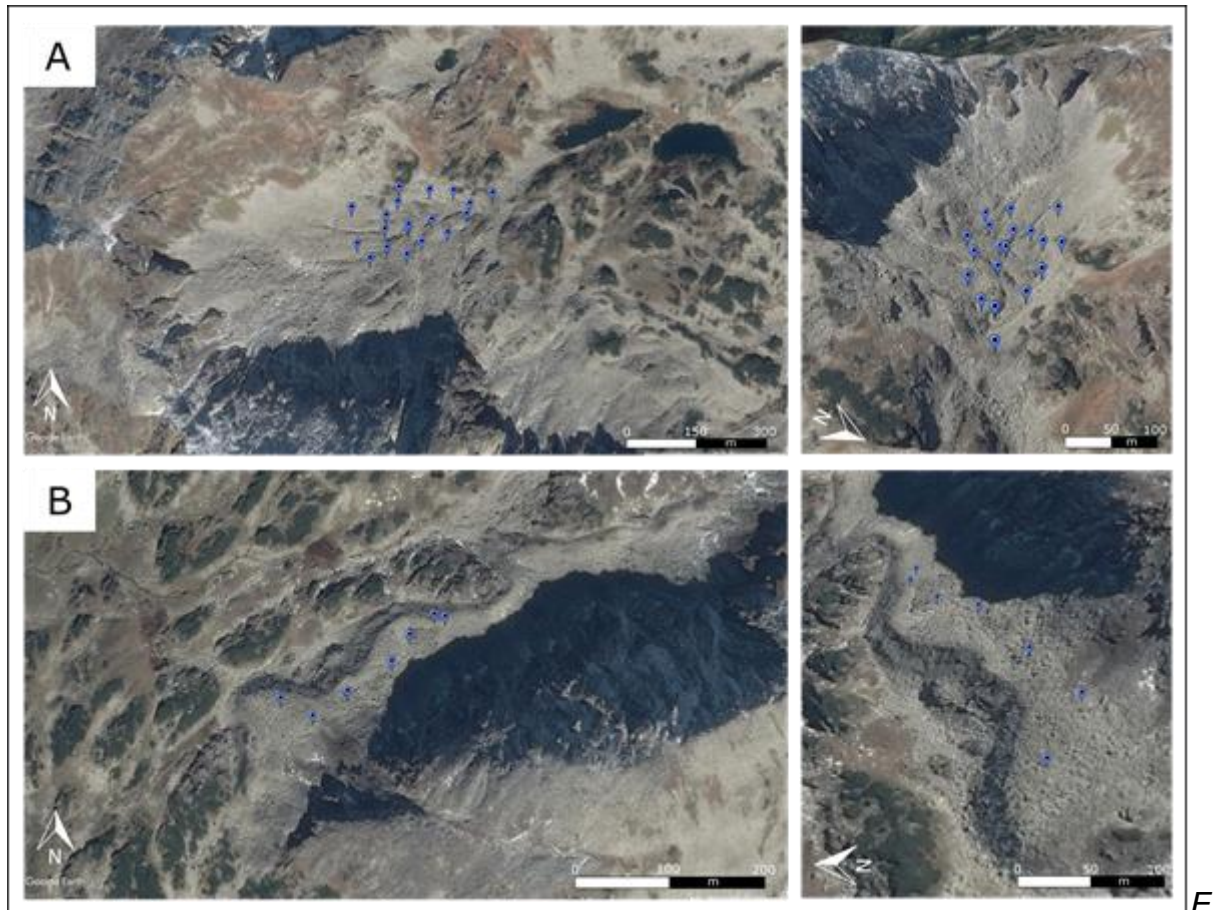

Figure 3.4.1   The distribution of GNSS measurement points (2019 survey) on the Judele (A) and Peleaga (B) rock glaciers (source of the background images: Google Earth, 16.11.2014, 2020 CNES/Airbus).
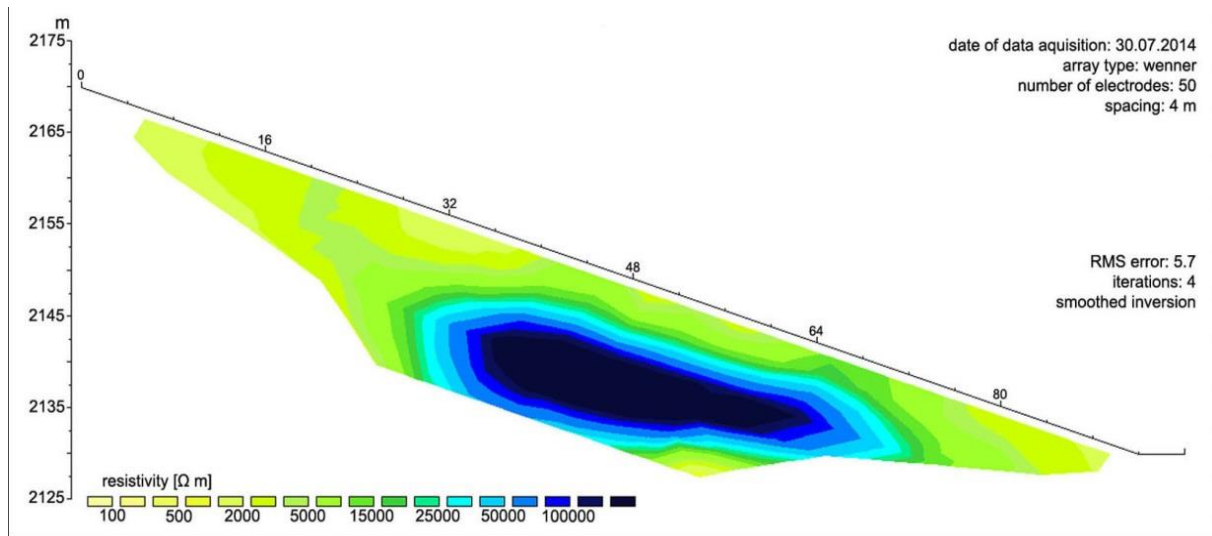
Figure 3.4.2 Example of a longitudinal ERT profile on Upper Pietricelele rock glacier (after Onaca et al., 2015).

3.4.3 Match Up Analyses

Introduction

The measured annual displacement rates (ADR) of the rock glaciers are extremely low in the central part of the Retezat Mountains, compared to other mountainous regions studied. Our analysis revealed that the highest annual displacement rates are only around 1 cm/yr, but in general only small parts of the investigated rock glaciers exhibit this pattern of deformation. In only two cases, the InSAR analysis provided maximum displacements rates between 1 and 2 cm/yr (Galeşu and Valea Rea 1 rock glaciers). 14 rock glaciers in the central part of the Retezat Mountains exhibit maximum annual displacement rates between 0.5 and 1 cm/yr, whereas the rest of 32 rock glaciers show insignificant displacements (below 0.5 cm/yr) (Figure 3.4.3). However, stable areas were also detected within the rock glacier outlines, suggesting that the dynamics of the rock glaciers are restricted to those parts where permafrost occurs.
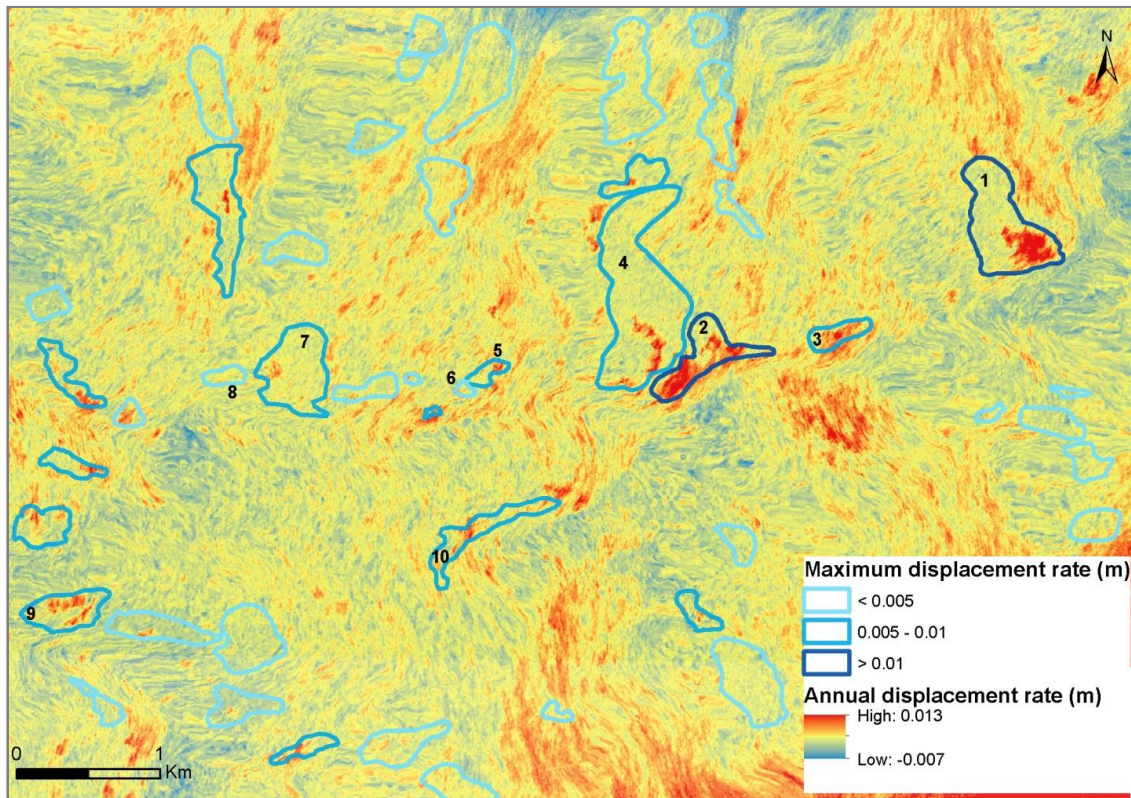
Figure 3.4.3 Annual displacement rates in the central part of the Retezat Mountains and the outlines of the rock glaciers. See the highest values concentrated on rock glaciers 1 (Galeşu) and 2 (Valea Rea). Validation data are also available for rock glaciers 3 (Valea Rea 2), 4 (Valea Rea 3), 5 (Pietricelele 1), 6 (Pietricelele 2), 7 (Pietrele 1), 8 (Pietrele 2), 9 (Judele), 10 (Berbecilor).

Differential GPS measurements August 2019 – October 2019

GNSS measurements of 18 points over Judele rock glacier (A) and 8 points over Berbecilor (B) rock glacier (Figure 3.4.1) were carried out during two campaigns on 12 August 2019 and 14 October 2019. Due to the short time between the measurements and due to the relatively slow movement of the rock glaciers the results showed no movement or very small movement, up to 0.0248 m. However, the instrumental error for our measurement condition is ±0.05 m (Figure 3.4.4). Thus, we consider the displacement measurements to be unreliable and we did not use them so far as data for absolute quality assessment.
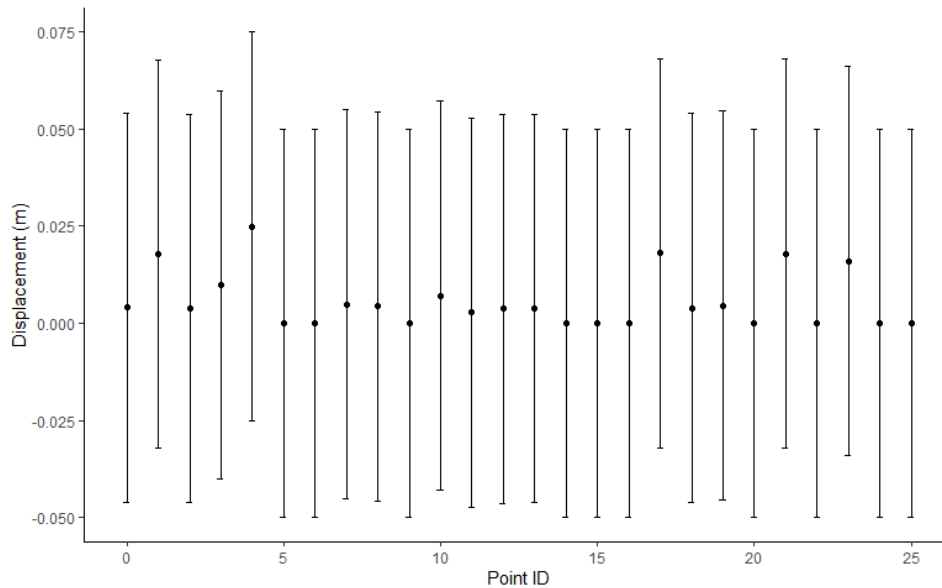
Figure 3.4.4   Displacement measurements over the Judele rock glacier (A) and 8 points over Berbecilor (B) rock glacier (see Figure 3.4.5) using a differential GPS and instrumental error.

Multi-annual in-situ velocity measurements 2008-2009 and 2012-2014

In the past, ADR were also compared from total stations surveys (Vespremeanu-Stroe et al., 2012; Popescu, 2015). The measurements of movement were performed between 2008 and 2009 at the Pietrele 1 site (Figure 3.4.5) and between 2012 and 2014 at the Judele site (Figure 3.4.6) by researchers from Bucharest University, but the results are inconsistent. At Pietrele 1 site, the displacements in the eastern part of the rock glacier ranged between 2 and 6 cm/yr. A repeated survey performed in 2013 revealed considerably lower displacement values in this area and chaotic patterns of horizontal displacements, leading to the conclusion that permafrost is unlikely here (Popescu, 2015). The 2-years horizontal rates of displacement at the Judele site ranged between 1.9 and 8.6 cm. Surprisingly, the frontal part of the rock glacier, where our previous investigations revealed the unlikely presence of permafrost, experienced relatively high displacements (between 3 and 4 cm/yr) (Popescu, 2015). More recently, lower ADR values (around 1-2 cm/yr) were presented by Popescu et al. (2019) for this rock glacier after some corrections of the initial data were performed. The velocity of Valea Rea 3 rock glacier was also assessed by Vespremeanu-Stroe et al. (2012), but the results of the total station survey between 2008 and 2009 were not clearly represented. Regarding this, a comment in this study reveals that the movement rates in the active parts of Pietrele and Valea Rea range between 2 and 8 cm/yr, but there is no map displayed.

Figure 3.4.5   Annual displacement rates based on InSAR analysis (Sentinel-1) (a) and geodetic surveys between 2008 and 2009 (b) (after Vespremeanu-Stroe et al., 2012) at Pietrele 1 rock glacier.

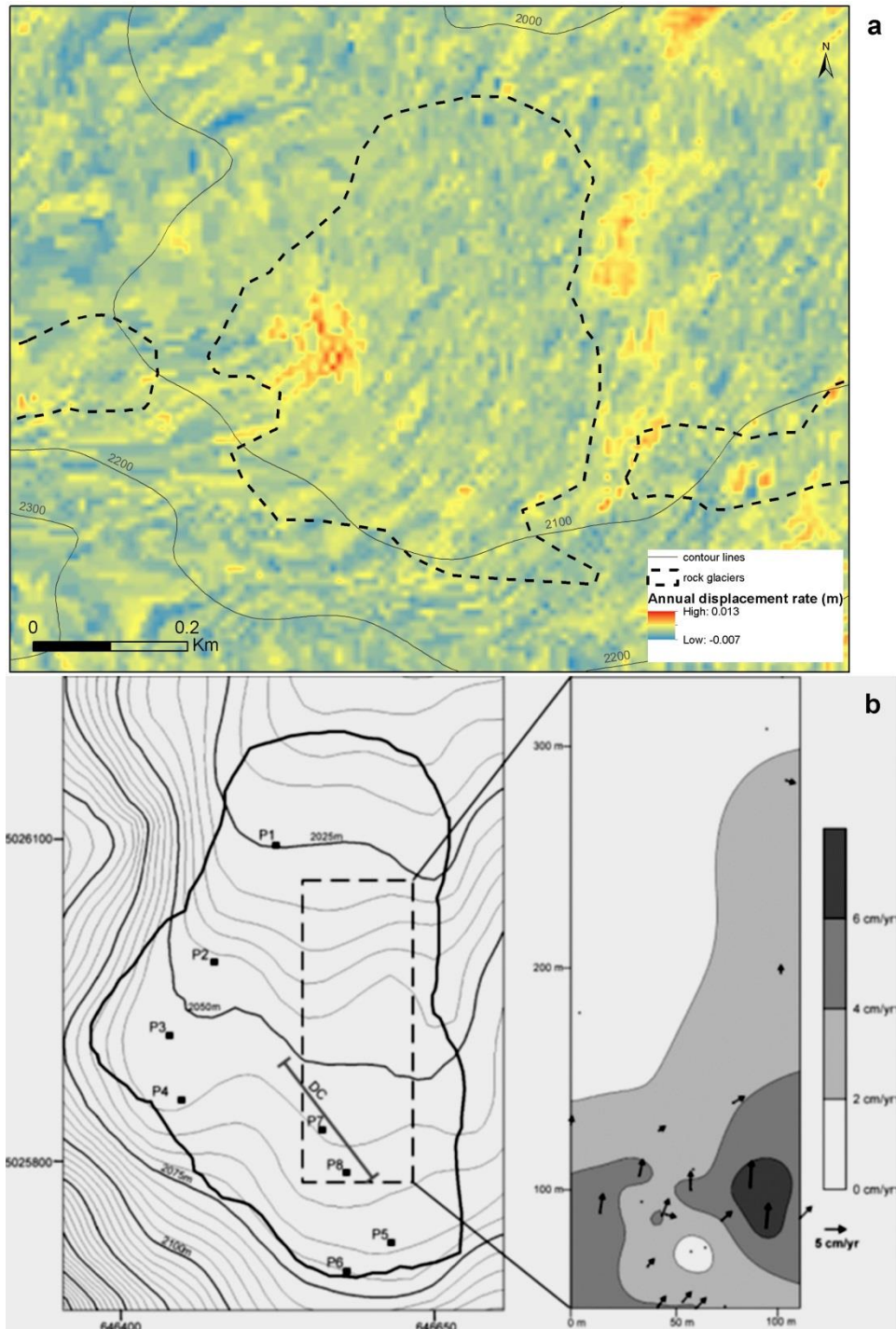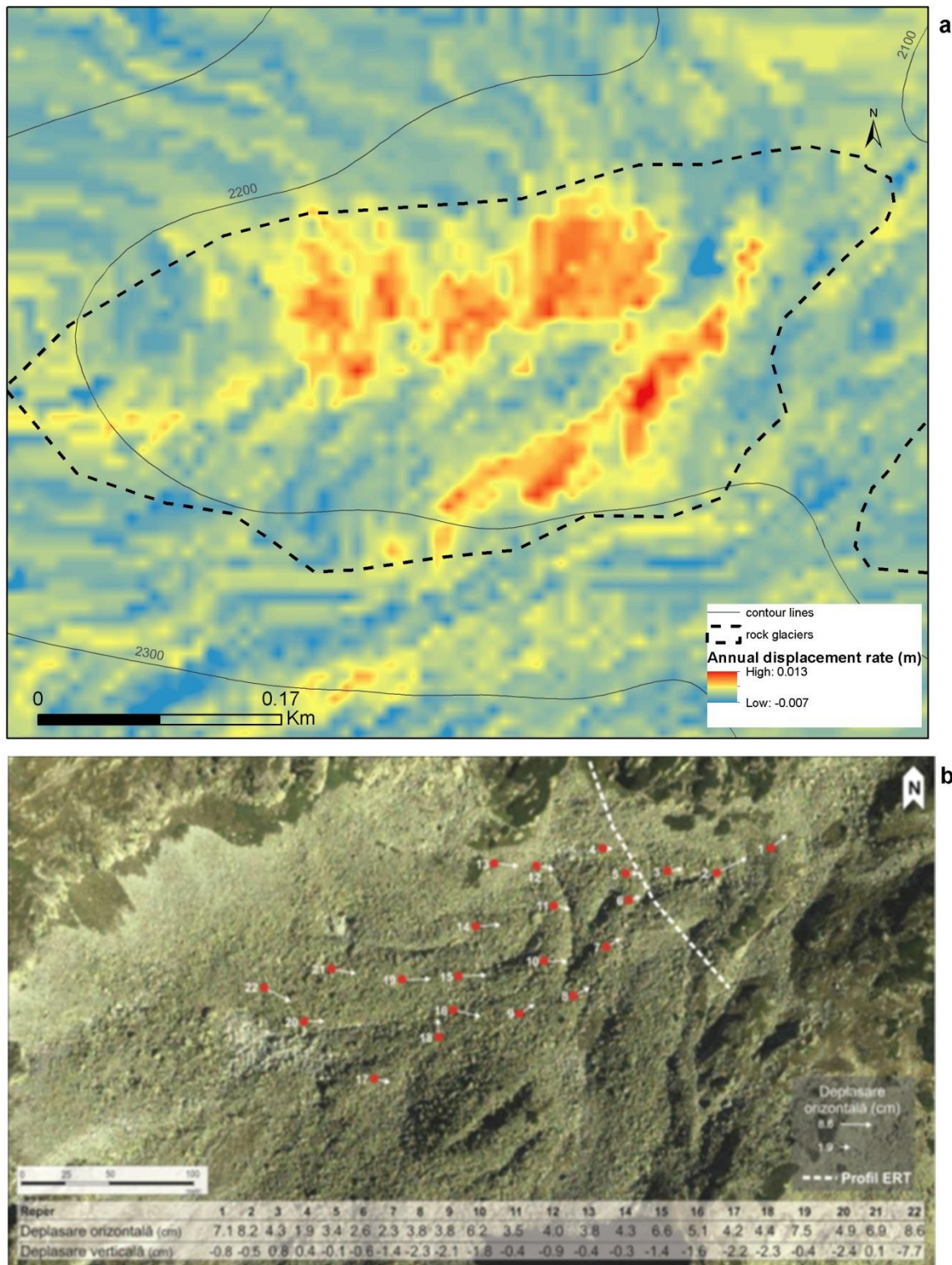*Figure 3.4.6 Annual displacement rates based on InSAR analysis (Sentinel-1) (a) and geodetic surveys between 2012 and 2014 (b) (after Popescu, 2015) at the Judele rock glacier. Horizontal and vertical displacement rates are displayed in the inset table.*

Geophysical surveys

The existing geophysical data were synthetized and are displayed in Figures 3.4.7 and 3.4.8. It appears that either Electrical Resistivity Tomography or Ground Penetrating Radar detected patches of ice-containing permafrost in specific parts of the rock glaciers. In some cases, there is a good correspondence between ADR and the occurrence of permafrost, whereas in other cases the presence of permafrost does not correspond with the areas characterized by the highest deformations.
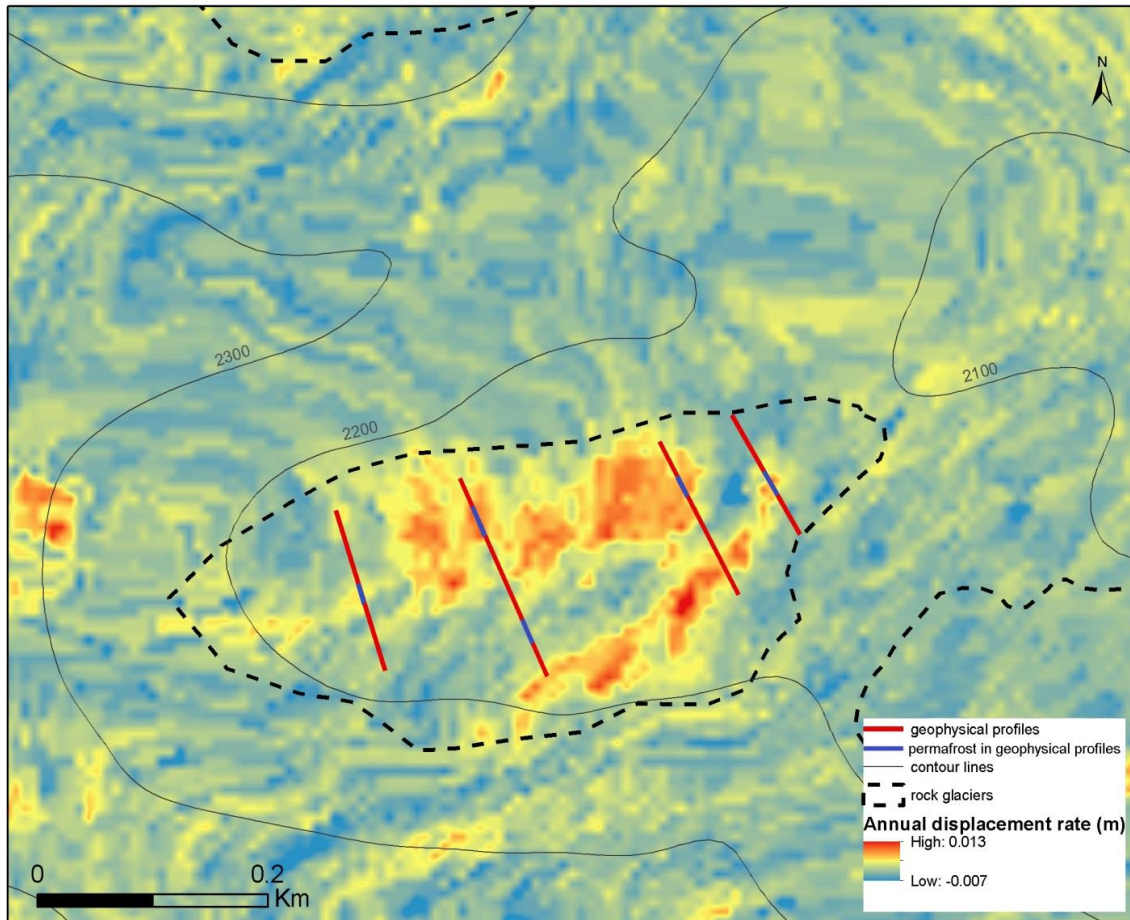

Figure 3.4.7   Annual displacement rates (Sentinel-1) of Judele rock glacier and the synthesis of permafrost distribution based on geophysical profiles.
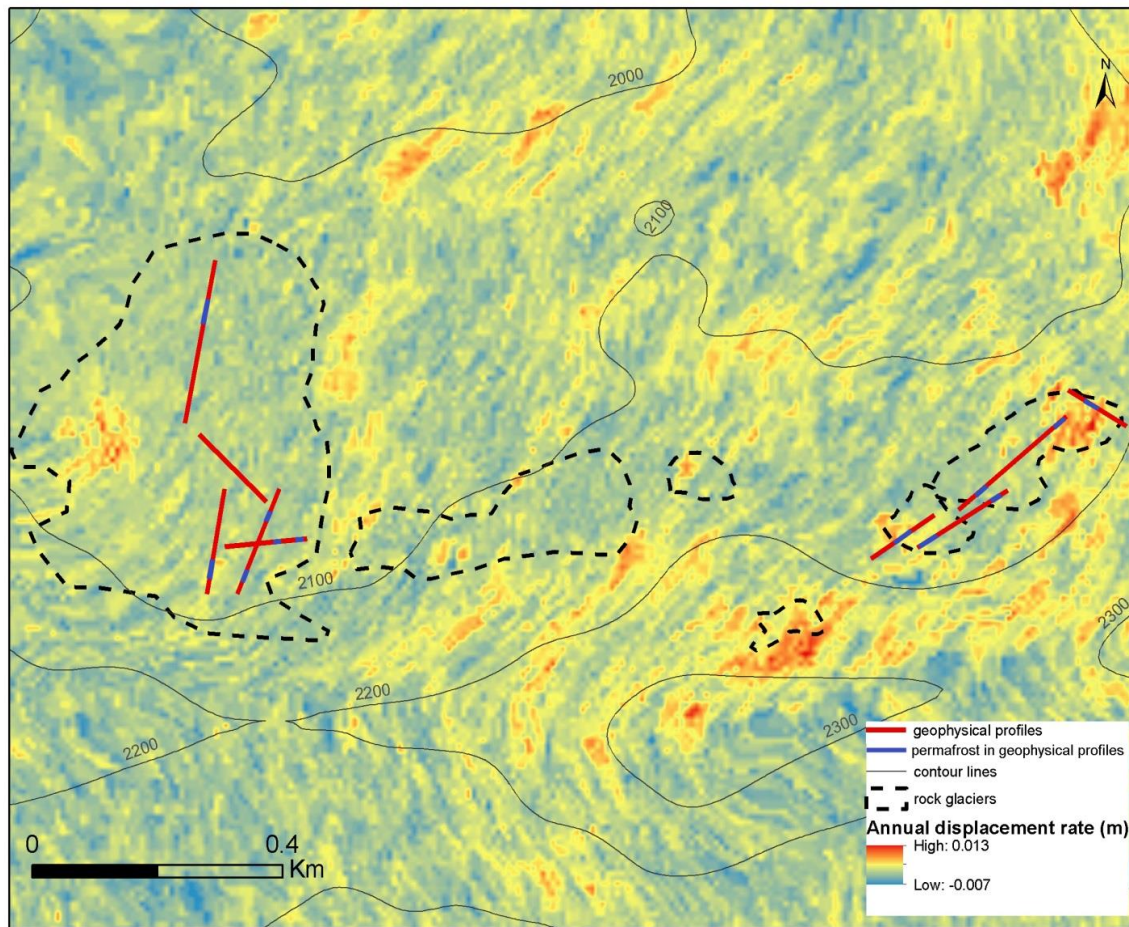
Figure 3.4.8   Annual displacement rates (Sentinel-1) and the synthesis of permafrost distribution in the Pietrele, Pietricelele 1 and Pietricelele 2 rock glaciers based on geophysical profiles.

GST in-situ measurements

Considering the existing ground surface temperature (GST) records, we noticed that permafrost occurrence is limited to several sites where the ground cooling is enhanced by the porous coarse block surfaces. At Galeșu rock glacier, three thermistors are located in the south-eastern part of the landform and all three reveal a GST regime typical for permafrost sites. In this case, there is a very good correspondence with the ADR since this part of the rock glacier experiences the highest ADR in the central part of Retezat Mountains (Figure 3.4.9). At Valea Rea 1, where also ADR values greater than 1 cm/yr were calculated, there is a very good correspondence with the likely presence of permafrost based on GST records (Figure 3.4.10). At Valea Rea 2 and 3 rock glaciers, the sites with probable permafrost correspond with surfaces characterized by ADR values between 0.5 and 1 cm/yr (Figure 3.4.10). On the contrary, at Pietrele and Pietricelele valleys the correspondence between ADR values and permafrost occurrence is not so evident (Figure 3.4.11). However, in the western part of Pietrele, eastern part of Pietricelele 1 and western extremity of Pietricelele 2, where permafrost is likely to occur, medium displacements were captured by the InSAR analysis (Figure 3.4.11). At Judele, three thermistors revealing permafrost are located at sites with ADR values higher than 0.5 cm/yr (Figure 3.4.12).

Figure 3.4.9 Annual displacement rates (Sentinel-1) and the likelihood of permafrost in the Galeşu rock glacier based on thermistors records.

Figure 3.4.10 Annual displacement rates (Sentinel-1) and the likelihood of permafrost in the Valea Rea Valley based on thermistors records.

Figure 3.4.11 Annual displacement rates (Sentinel-1) and the likelihood of permafrost in the Pietrele Valley based on thermistors records.

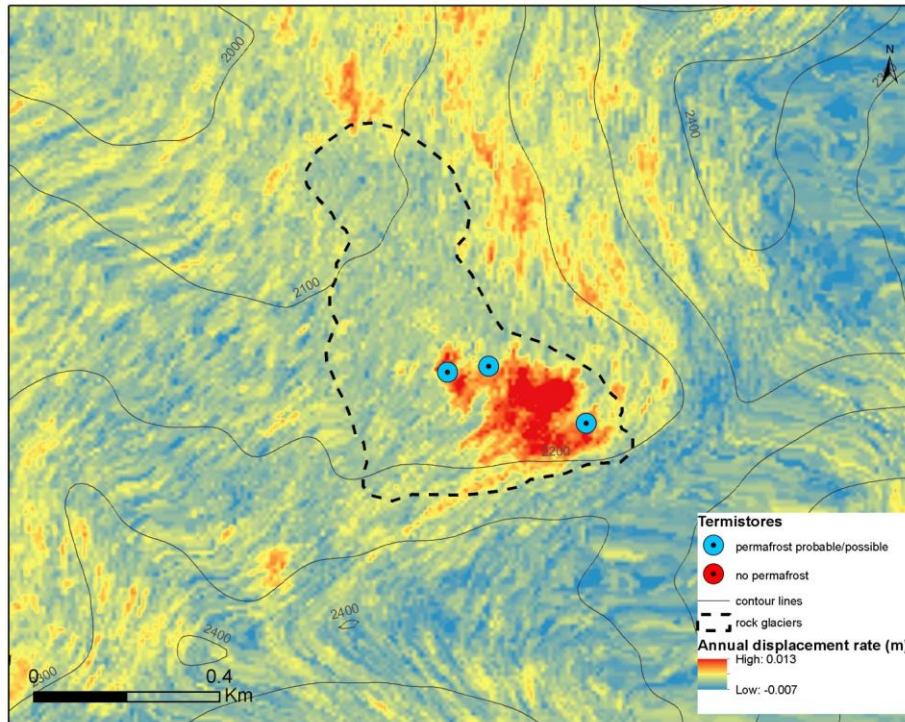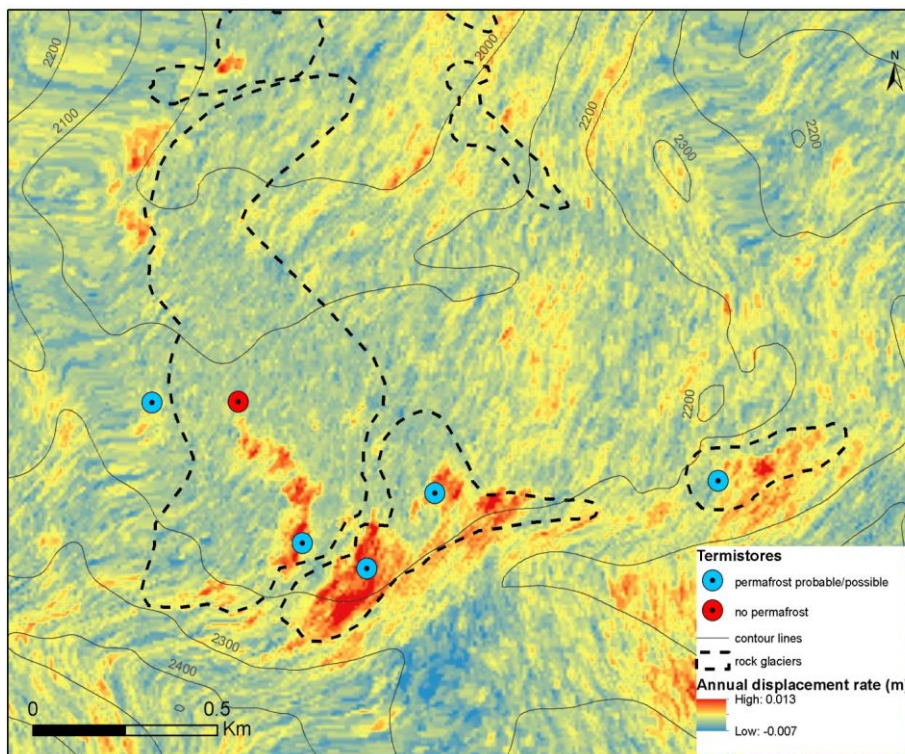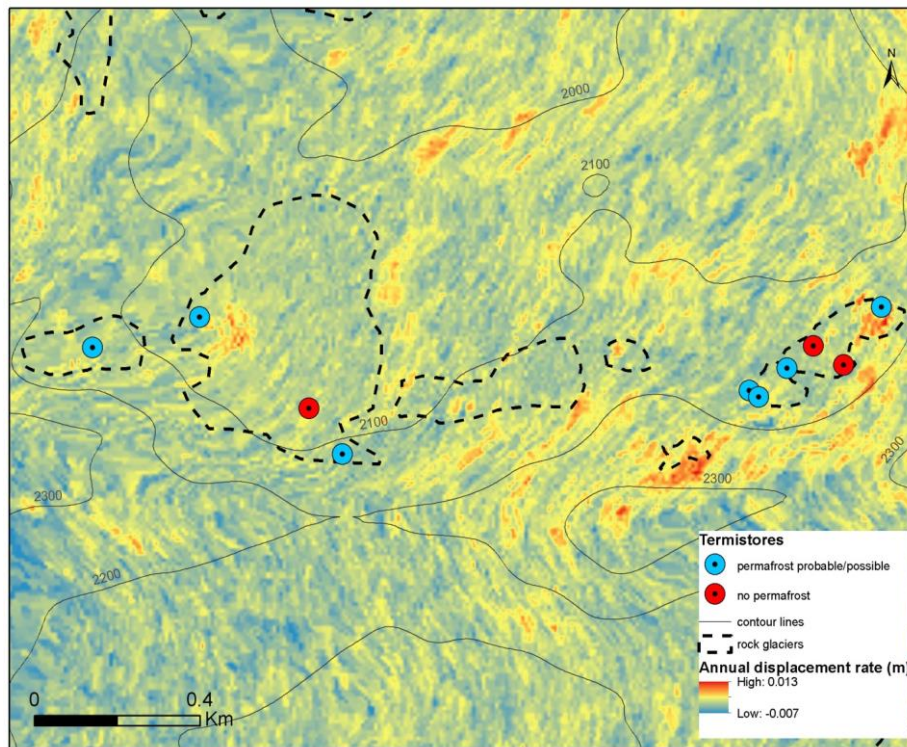*Figure 3.4.12 Annual displacement rates (Sentinel-1) and the likelihood of permafrost at the Judele rock glacier based on thermistors records.*

Standard deviation of displacement rates

As a relative quality measure of the rock glacier velocities using Sentinel-1 data only, the standard deviation of the measured displacement rates in a least squares sense is illustrated in Figure 3.4.13. A low standard deviation is an indication of matching measurements from independent Sentinel-1 interferograms; thus, it can be used as a measure of quality of the results, subject to the limitations of the sensor and the InSAR technique (assuming the sensor functions correctly and the InSAR technique measures actual velocities).

0   0.005

Figure 3.4.13 Measurement noise standard deviation of Sentinel-1 data for selected rock glaciers. Red points indicate rock glacier locations with known dynamics and the red star indicates the location of both GPS and InSAR references.

Comparison between displacement measurements from multiple satellite sensors

As another relative quality measure, the velocity maps derived from Sentinel-1 using the InSAR stacking method and from ALOS-2 PALSAR-2 using standard InSAR, covering roughly the same period, were compared in Figures 3.4.14 and 3.4.15. In spite of the different viewing geometries (descending for Sentinel-1 and ascending for ALOS-2 PALSAR-2), a generally good correspondence

between the two maps is observed, with the fastest moving parts of the rock glaciers depicted with both sensors.

Figure 3.4.14 Example for ALOS-2 PALSAR-2 interferogram (20140908 - 20191014).

Figure 3.4.15 Example for Sentinel-1 InSAR stacking results (20150831 - 20191009).

Comparison with the permafrost distribution map

Due to the different nature of the permafrost distribution map and of the annual displacement rates determined from Sentinel-1, we considered that a visual, expert based, comparison of the two maps is more suited than a quantitative analysis. For this, we have selected four rock glaciers in the central part of the Retezat Mountains (figure 3.4.16). Permafrost has been modeled to exist inside and outside of rock glaciers. For the permafrost inside of rock glaciers, in the selected area, there is a good overlay with the areas found to have movement by the Sentinel-1 derived velocities maps. This can be observed in figure 3.4.16 for the SE part of Galeşul RG (1), Valea Rea1 (2) and Valea Rea2 (3) rock glaciers and the southern part of Valea Rea3 RG (4).
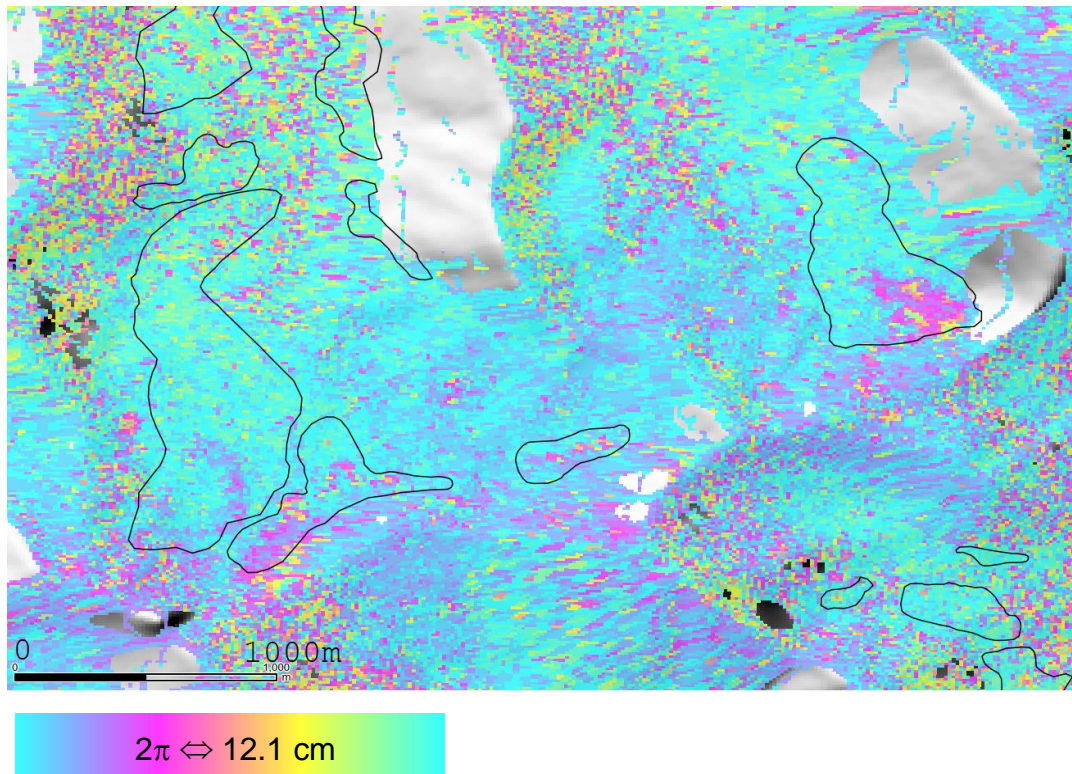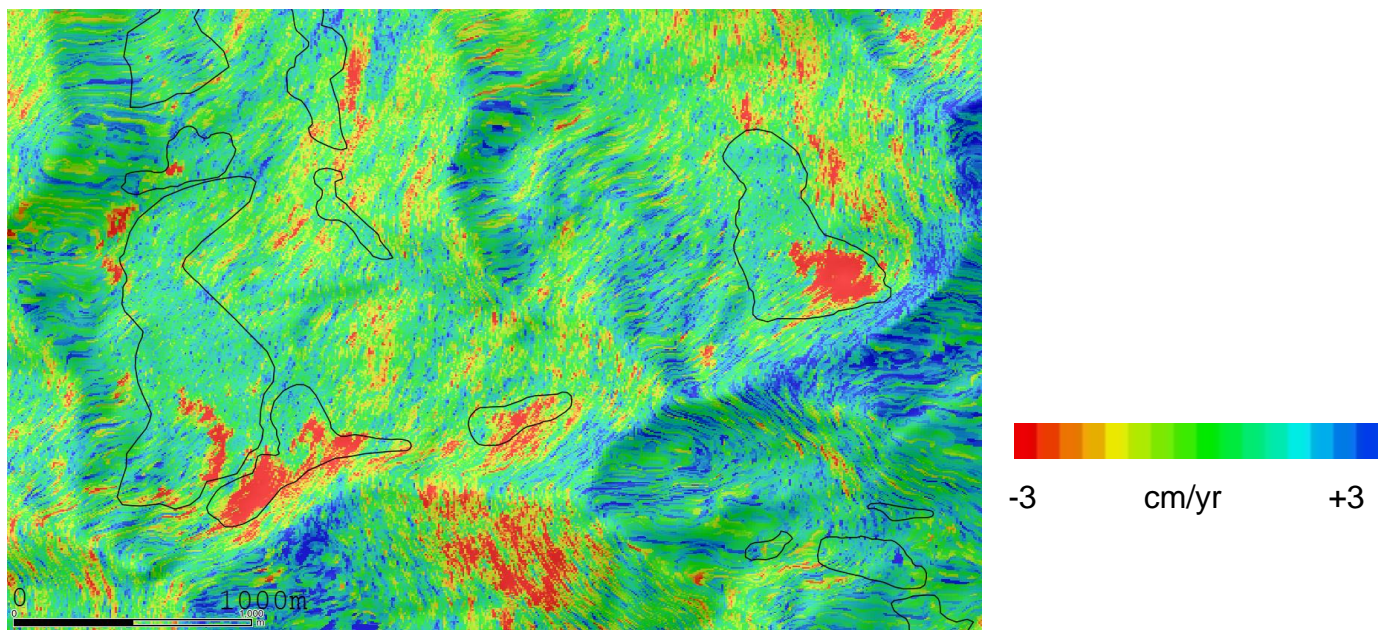

Figure 3.4.16 Comparison between the modelled permafrost distribution map (left) and the velocities map derived from Sentinel-1 using the InSAR stacking method (right) for four rock glaciers: 1 - Galeşu, 2 - Valea Rea, 3 - Valea Rea2, 4 - Valea Rea3.

Conclusions

As an absolute validation for the trends in rock glaciers velocity in the Romanian Carpathians, GNSS measurements of 18 points over Judele rock glacier and eight points over Peleaga rock glacier in Retezat mountains were carried out during two campaigns on 12 August and 14 October 2019. Due to the unique terrain settings and to the very slow movement of the rock glaciers, the validation using absolute measurements was considered unreliable as the error of the in-situ measurements is greater than the measured distance. The quality of the final results was thus estimated in a least-squares sense from multiple Sentinel-1 measurements covering overlapping periods of time between 2015-2019 and extrapolated to yearly displacement rates using the InSAR stacking technique. Velocity trends extracted in this way show a low noise level and suggest better than centimetric accuracy of the glacier velocity measurements. In addition, geophysical and temperature measurements are indirectly linked

to the velocity maps, as they are indicators of permafrost presence/absence. We found that the best methods for validation of the velocity maps, under present conditions, are relative measurements and expert based visual comparison between permafrost map and velocity maps developed using different satellite images and different methods. The standard deviation of the measured displacement rates, used as a relative measurement of error, shows relatively low values for the area of interest and visual comparison with ALOS-2 PALSAR-2 interferograms and the permafrost map showed a good match between them for four rock glaciers.

4 Permafrost distribution model at regional scale

4.1 Methods for Quality Assessment

The performance of each model was evaluated using the AUC (area under the curve) metric. The AUC is obtained by plotting all possible sensitivity (true positive) rates against 1-sensitivity (false positive) rates and returns values between 0.5 (no discrimination between presence/absence) and 1 (perfect discrimination) (Hosmer and Lemeshow, 2000). The AUC values are computed using the ROCR package (Sing et al., 2005). The AUC offers the possibility of finding the best value at which a threshold can be chosen to classify the continuous values of permafrost probability in order to produce a map with two classes (permafrost and non-permafrost areas).

The confusion matrix is a table layout that allows for the visualization of the classification results against the validation data. It is used after the permafrost probability map has been classified into permafrost and non-permafrost areas.

4.2 Reference Data

The data used for product validation of the permafrost probability map consists of 76 data points from the central area of Retezat Mountains. The data is obtained through BTS measurements and GST measurements performed with iButtons, from which only the winter equilibrium temperature was used.

<u>BTS method</u>

The Bottom Temperature of Snow Cover (BTS) refers to temperature measured in late winter at the snow/ground interface. The BTS data was classified into presence/absence of permafrost using the -3°C cut off value (Haeberli, 1973). The BTS method is one of the most efficient for permafrost probability assessment in regions with a sufficient onset of snow accumulation during the winter. This method was introduced by Haeberli (1973) and since then it has subsequently been used in different alpine regions, such as the Alps (Hoelzle, 1992), Scandinavian Alps (Ødegård et al. 1996) Romanian Carpathians (Urdea, 1993), Tatra Mountains (Mościcki and Kędzia, 2001), the Pyrenees (Julián and Chueca, 2007), Sierra Nevada (Tanarro et al., 2001), Rila and Pirin Mountains (Onaca et al., 2020), Daisetsu Mountains (Ishikawa and Hirakawa, 2000) etc. The method is based on the observation that in late winter (February-April), under a deep snow cover a thermal equilibrium occurs at the base of the snow cover, due to the insulating effect of persistent snow. Since in late winter the temperatures at the snow-ground interface will remain relatively stable, the BTS values will reflect winter thermal conditions within the ground. Thus, according to 'rules of thumb' (Haeberli, 1973) where BTS values are below -3°C permafrost is probable, values of -2 to -3°C indicate that permafrost is possible whereas BTS values higher than -2°C suggest that permafrost is improbable (Hoelzle, 1992).

BTS values are strictly dependent on the history and duration of the snow cover at the measurement site. A thick snow cover of at least 80-100 cm (Haeberli, 1973) is necessary to persist for minimum two weeks before the date of measurements to provide a sufficient thermal insulation of the ground

(Schoeneich, 2011). The BTS measurements were realized using two lightweight 2.6 m long BTS probes equipped with digital thermometers (0.5°C precision). The location of each BTS point was obtained using a handheld GPS (Garmin 76 CSx) in the field. All the measurements were collected in late March 2019 when the snow thickness was greater than 100 cm at all the sites.

Based on the statistical relationships between BTS values and different predictor variables (e.g., elevation, slope, profile curvature, solar radiation, NDVI etc.) the distribution of permafrost in different areas was modeled (Gruber and Hoelzle, 2001; Lewkowicz and Ednie, 2004; Julián and Chueca, 2007; Ardelean et al., 2015).

Ground Surface Temperature (GST)

In the last two decades, continuous in-situ GST measurements in periglacial regions were intensively used to assess if the microclimatic conditions at the surface of the ground are suitable for hosting permafrost. Due to their low price and fair reliability, iButtons are frequently preferred in studies related with mapping permafrost distribution in high mountains (Haberkorn et al., 2015). In the Retezat Mountains we have used 8 iButtons DS1922L miniature thermistors (0.5°C accuracy; 0.06°C resolution; -40…+80°C temperature range). All the thermistors were set to record temperature data every two/four hours, since 1 September 2012. These miniature data loggers were distributed at the surface of several rock glaciers in the central part of Retezat Mountains and covered by debris to avoid heating by direct solar radiation (Gubler et al., 2011). The 'Zero curtain' interval was used to indirectly calibrate the sensors. To delineate between permafrost and non-permafrost areas we used the winter equilibrium temperature and considered the aforementioned BTS thresholds.

The permafrost predicted probability is the value of the model result in each of the validation points. The classification of the predicted probability is done using the cut off value of 0.7985 based on the AUC (see 4.1).

Table 4.2.1 Available BTS (Bottom Temperature of Snow Cover) measurements and permafrost distribution model results.

ID	BTS	BTS_class (1 – presence, 0 – absence)	Predicted_probability	Predicted_class (1 – presence, 0 – absence)
1	-4	1	0.912	1
2	-4.7	1	0.912	1
3	-3.2	1	0.912	1
4	-3	1	0.861	1
5	-2.5	0	0.84	1
6	-3.9	1	0.96	1
7	-2.8	0	0.921	1
8	-2.2	0	0.768	0
9	-1.2	0	0.792	0

10	-2.9	0	0.958	1
11	-1.7	0	0.635	0
12	-1.5	0	0.684	0
13	-3.2	1	0.911	1
14	-3.8	1	0.716	0
15	-5.1	1	0.888	1
16	-3.1	1	0.977	1
17	-1.2	0	0.622	0
18	-5.2	1	0.886	1
19	-4.7	1	0.861	1
20	-0.6	0	0.703	0
21	-1	0	0.682	0
22	-3.7	1	0.944	1
23	-3.9	1	0.868	1
24	-3.4	1	0.823	1
25	-4	1	0.894	1
26	-2.5	0	0.799	1
27	-3.2	1	0.834	1
28	-1.5	0	0.432	0
29	-1.7	0	0.507	0
30	-0.7	0	0.797	0
31	-1.1	0	0.403	0
32	-1.3	0	0.33	0
33	-1.4	0	0.657	0
34	-2.1	0	0.21	0
35	-4.1	1	0.98	1
36	-4.4	1	0.873	1
37	-5.2	1	0.981	1
38	-2.4	0	0.659	0
39	-3.5	1	0.87	1
40	-4.1	1	0.952	1
41	-2.1	0	0.521	0
42	-3.2	1	0.971	1
43	-0.5	0	0.465	0
44	-2	0	0.604	0
45	-0.9	0	0.756	0
46	-2.2	0	0.792	0
47	-4	1	0.902	1
48	-5.4	1	0.978	1
49	-3.2	1	0.985	1
50	-2.7	0	0.819	1

51	-2.6	0	0.985	1
52	-3.1	1	0.872	1
53	-2.3	0	0.773	0
54	-0.7	0	0.508	0
55	-2.1	0	0.616	0
56	-0.4	0	0.354	0
57	-0.5	0	0.705	0
58	-0.2	0	0.464	0
59	-0.9	0	0.088	0
60	-0.8	0	0.258	0
61	-1.6	0	0.2	0
62	-1.8	0	0.307	0
63	-1.4	0	0.445	0
64	-3.1	1	0.842	1
65	-2.1	0	0.429	0
66	-3.2	1	0.949	1
67	-1.8	0	0.116	0
68	-3.3	1	0.877	1
69	-3.2	1	0.971	1
70	-1.4	0	0.294	0
71	-1.7	0	0.181	0
72	-1.8	0	0.237	0
73	-1.2	0	0.472	0
74	-1.9	0	0.426	0
75	-0.8	0	0.404	0
76	-0.9	0	0.405	0

4.3 Match Up Analyses

The AUC graph and values were computed based on 76 validation points, independent from the training data, located in the central area of the Retezat Mountains. Because the permafrost in the Southern Carpathians is patchy and occurs only under site-specific conditions, the validation points are not evenly distributed in the modelled region but are located in a study area at sites with known permafrost or in their vicinity. By employing this validation strategy, we aim to have a more accurate AUC value and cut-off value, by avoiding having a high number of validation points in areas with low permafrost probability and thus artificially increasing the accuracy of the model.
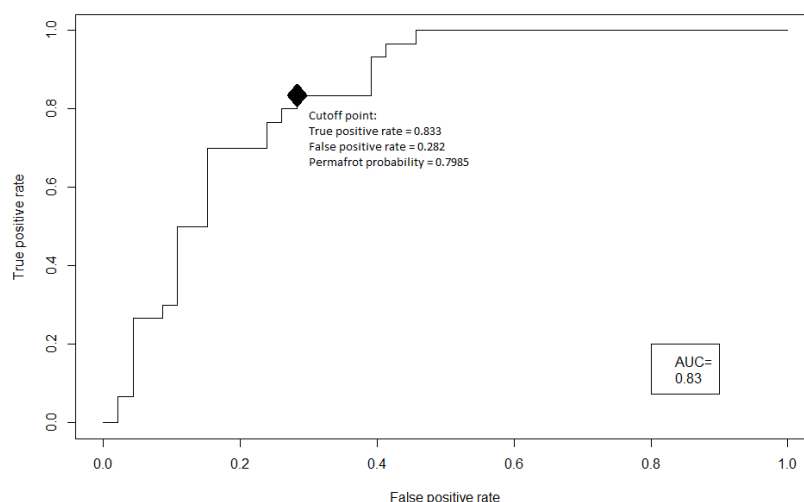
Figure 4.3.1   AUC (Area under the curve) results for the permafrost prediction model in the southern Carpathians .

The AUC value for the permafrost prediction model in the Southern Carpathians is AUC = 0.83 which is in the range of a very good model. For computing the AUC values the predicted probability and BTS_class value from Table 1 has been used.

Because the histogram of the permafrost prediction map is strongly skewed to the left, most of the values are smaller than 0.5 and the AUC curve is flat in its right side, with TPR=1 and FPR between 0.46 and 1. Thus, if the cut-off point would be selected in this area, the model will, most likely, produce an overestimation of the size of permafrost areas.

Based on the AUC curve the cut-off point has been chosen to have a high value of TPR and an as small as possible FPR. For the point on the curve with a TPR=0.833 and an FPR=0.282, the cut off value is 0.7985. This value was further been used to classify the permafrost probability prediction into a permafrost extent map with presence/absence values.

The resulting classified map has been evaluated using the BTS_class and Predicted_class values from Table 1 by using a confusion matrix (Table 4.3.1). It shows that out of 46 points where measurements showed permafrost absence 40 were correctly classified and out of 30 points where permafrost presence was measured 29 were correctly classified. In total 69 points (90%) out of 76 had been correctly classified.

Table 4.3.1   *Confusion matrix for permafrost presence (1) /absence (0).*

		BTS (measured)	
		0	1
Predicted values	0	40	1
	1	6	29

The classified map has also been assessed based on expert knowledge of the study area by the team from WUT.

5 References

5.1 Bibliography

Ardelean, A.C., Onaca, A.L., Urdea, P., Șerban, R.D., Sîrbu, F., 2015. A first estimate of permafrost distribution from BTS measurements in the Romanian Carpathians (Retezat Mountains). Géomorphologie: relief, processus, environnement, 2, 4, 297-312.

Bartsch, A., Grosse, G., Kääb, A., Westermann, S., Strozzi, T., Wiesmann, A., Duguay, C., Seifert, F. M., Obu, J., Goler, R., GlobPermafrost – How space-based earth observation supports understanding of permafrost. Proc. 'Living Planet Symposium 2016', Prague, Czech Republic, 9–13 May 2016 (ESA SP-7 40, August 2016), pp. 6.

Blikra, L. H., Henderson, I., Nordvik, T. 2009. Faren for fjellskred fra Nordnesfjellet i Lyngenfjorden, Troms. [In Norwegian]. Norges geologiske undersøkelse (NGU) Report 2009.026. https://hdl.handle.net/11250/2664691.

Blikra, L. H., Christiansen, H. H., Kristensen, L., Lovisolo, M. 2015. Characterization, geometry, temporal evolution and controlling mechanisms of the Jettan Rock-Slide, Northern Norway. In: Engineering Geology for Society and Territory-Volume 2 (pp. 273-278), Springer, Cham.

Blöthe JH, Halla C, Schwalbe E, Bottegal E, Liaudat DT and Schrott L Surface velocity fields of active rock glaciers and ice-debris complexes in the Central Andes of Argentina. Earth Surf. Process. Landf. n/a(n/a) (doi:https://doi.org/10.1002/esp.5042)

Böhme, M., Bunkholt, H.S.S., Oppikofer, T., Dehls, J.F., Hermanns, R.L., Eriksen, H.Ø., Lauknes, T.R. and Eiken, T., 2016. June. Using 2D InSAR, dGNSS and structural field data to understand the deformation mechanism of the unstable rock slope Gamanjunni 3, northern Norway. In Landslides and Engineered Slopes: Experience, Theory and Practice: Proceedings of the 12th International Symposium on Landslides (Napoli, Italy, 12–19 June 2016): Rome, Associazione Geotecnica Italiana (pp. 443-449).

Böhme, M., Hermanns, R. L., Gosse J., Hilger, P., Eiken, T., Lauknes, T. R., Dehls, J. F., 2019. Comparison of monitoring data with paleo–slip rates: cosmogenic nuclide dating detects acceleration of a rockslide. Geology, 47, 1–4, https://doi.org/10.1130/G45684.1/4655152/g45684.pdf, 2019.

Christiansen, H.H, Etzelmüller, B., Isaksen, K., Juliussen, H., Farbrot, H., Humlum, O., Johansson, M., Ingeman-Nielsen, T., Kristensen, L., Hjort, J, Holmlund, P., Sannel, A.B.K., Sigsgaard, C., Åkerman, H.J., Foged, N., Blikra, L.H., Pernosky, M.A. and Ødegård, R., 2010. The Thermal State of Permafrost in the Nordic area during the International Polar Year 2007-2009. Permafrost and Periglacial Processes, 21, 156-181.

Delaloye, R., Lambiel, C. and Gärtner-Roer, I., 2010. Overview of rock glacier kinematics research in the Swiss Alps: seasonal rhythm, interannual variations and trends over several decades. Geographica Helvetica, 65(2), 135–145.

Dehls, J. F., Larsen, Y., Marinkovic, P., Lauknes, T. R., Stødle, D., & Moldestad, D. A., 2019. INSAR. No: A National Insar Deformation Mapping/Monitoring Service In Norway--From Concept To Operations. In IGARSS 2019-2019 IEEE International Geoscience and Remote Sensing Symposium (pp. 5461-5464). IEEE.

Eriksen, H. Ø., Lauknes, T. R., Larsen, Y., Corner, G. D., Bergh, S. G., Dehls, J., Kierulf, H. P. 2017a. Visualizing and interpreting surface displacement patterns on unstable slopes using multi-geometry satellite SAR interferometry (2D InSAR), Remote Sens. Environ., 191, 297–312. https://doi.org/10.1016/j.rse.2016.12.024.

Eriksen, H. Ø., Bergh, S. G., Larsen, Y., Skrede, I., Kristensen, L., Lauknes, T. R., Blikra, L. H., Kierulf, H. P., 2017b. Relating 3D surface displacement from satellite-and ground-based InSAR to structures and geomorphology of the Jettan rockslide, northern Norway, Norw. J. Geol., 97(4), 283–303. https://doi.org/10.17850/njg97-4-03, 2017b.

Eriksen, H.Ø., Rouyet, L., Lauknes, T.R., Berthling, I., Isaksen, K., Hindberg, H., Larsen, Y. and Corner, G.D., 2018. Recent acceleration of a rock glacier complex, Ádjet, Norway, documented by 62 years of remote sensing observations. Geophysical Research Letters, 45(16), pp.8314-8323.

Gubler, S., Fiddes, J., Keller, M., & Gruber, S., 2011. Scale-dependent measurement and analysis of ground surface temperature variability in alpine terrain. The Cryosphere, 5(2), 431-443.

Gruber, S., Hoelzle, M., 2001. Statistical modelling of mountain permafrost distribution: local calibration and incorporation of remotely sensed data. Permafrost and Periglacial Processes, 12(1), 69-77.

Haeberli, W., 1973. Die Basis Temperatur der winterlichen Schneedecke als möglicher Indikator für die Verbreitung von Permafrost. Zeitschrift für Gletscherkunde und Glazialgeologie, 9, 221-227.

Haeberli, W., Noetzli, J., Arenson, L., Delaloye, R., Gärtner-Roer, I., Gruber, S., Isaksen, K., Kneisel, C., Krautblatter, M., Phillips, M., 2010. Mountain permafrost: development and challenges of a young research field. Journal of Glaciology, 56(200), 1043-1058.

Haeberli, W., Hallet, B., Arenson, L., Elconin, R., Humlum, O., Kääb, A., Kaufmann, V., Ladanyi, B., Matsuoka, N., Springman, S., Vonder Mühll, D., 2006. Permafrost creep and rock glacier dynamics. Permafrost and Periglacial Processes 17 (3), 189–214.

Harris, C., Luetschg, M., Davies, M.C.R., Smith, F., Christiansen, H.H. and Isaksen, K., 2007. Field Instrumentation for Real-time Monitoring of Periglacial Solifluction. Permafrost and Periglacial Processes, 18, 105-114.

Harris, C., Arenson, L.U., Christiansen, H.H., Etzelmüller, B., Frauenfelder, R., Gruber, S., Haeberli, W., Hauck, C., Hölzle, M., Humlum, O., Isaksen, K., Kääb, A., Kern-Lütschg, M.A., Lehning, M., Hosmer D. W., Lemeshow S., 2000. Applied logistic regression. New York: Wiley.

Lewkowicz, A. G., & Ednie, M., 2004. Probability mapping of mountain permafrost using the BTS method, Wolf Creek, Yukon Territory, Canada. Permafrost and Periglacial Processes, 15(1), 67-80.

Matsuoka, N., Murton, J.B., Nötzli, J., Phillips, M., Ross, N., Seppälä, M., Springman, S.M., Vonder Mühll, D., 2009. Permafrost and climate in Europe: Monitoring and modelling thermal, geomorphological and geotechnical responses. Earth-Science Reviews, 92(3), 117-171.

Haberkorn, A., Phillips, M., Kenner, R., Rhyner, H., Bavay, M., Galos, S. P., & Hoelzle, M., 2015. Thermal regime of rock and its relation to snow cover in steep Alpine rock walls: Gemsstock, central Swiss Alps. Geografiska Annaler: Series A, Physical Geography, 97(3), 579-597.

Harris, C., Kern Luetschg, M., Christiansen, H.H. and Smith, F., 2011. The role of interannual climate variability in controlling solifluction processes, Endalen, Svalbard. Permafrost and Periglacial Processes, 22(3), pp.239-253.

Hoelzle, M., 1992. Permafrost occurrence from BTS measurements and climatic parameters in the Eastern Swiss Alps. Permafrost and Periglacial Processes, 3(2), 143-147.

Ishikawa, M., & Hirakawa, K., 2000. Mountain permafrost distribution based on BTS measurements and DC resistivity soundings in the Daisetsu Mountains, Hokkaido, Japan. Permafrost and Periglacial Processes, 11(2), 109-123.

Julián, A., & Chueca, J., 2007. Permafrost distribution from BTS measurements (Sierra de Telera, Central Pyrenees, Spain): assessing the importance of solar radiation in a mid-elevation shaded mountainous area. Permafrost and Periglacial Processes, 18(2), 137-149.

Kääb, A. and Vollmer M., 2000. Surface geometry, thickness changes and flow fields on creeping mountain permafrost: automatic extraction by digital image analysis.
Permafrost and Periglacial Processes,11, 315-326

Kääb, A., Isaksen, K., Eiken T. and Farbrot. H., 2002. Geometry and dynamics of two lobe-shaped rock glaciers in the permafrost of Svalbard. Norwegian Journal of Geography, 56, 152-160

Kääb, A., Strozzi T., Bolch T., Caduff R., Trefall H., Stoffel M., Kokarev A., 2021. Inventory and changes of rock glacier creep speeds in Ile Alatau and Kungöy Ala-Too, northern Tien Shan, since the 1950s. The Cryosphere. In press.

Matsuoka, M, Watanabe, T., Ikea, A, Christiansen, H. H., Humlum, O, Rouyet, L., 2019. Decadal-scale variability of polar rock glacier dynamics: accelerating due to warming? Presentation at the

Southern Hemisphere Conference On Permafrost (SouthCop), 4–14 December 2019, Queenstown, New Zealand.

Mościcki, J., Kędzia, S., Kotarba, A., 2001. Geomorphological and Geophysical Studies in a Subarctic Environment of Karkevagge Valley, Abisko Mountains, Northern Sweden. Bulletin of the Polish Academy of Sciences. Earth Sciences, 49(2), 123-135.

NGU. 2020. InSAR Norway, www.insar.no, map viewer: https://insar.ngu.no/.

Ødegård, R. S., Hoelzle, M., Vedel Johansen, K., & L. Sollid, J., 1996. Permafrost mapping and prospecting in southern Norway. Norsk geografisk tidsskrift-Norwegian Journal of Geography, 50(1), 41-53.

Onaca, A., Ardelean, F., Urdea, P., Magori, B., 2017. Southern Carpathian rock glaciers: inventory, distribution and environmental controlling factors, Geomorphology. 293, 391-404.

Onaca, A., Ardelean, A. C., Urdea, P., Ardelean, F., Sîrbu, F., 2015, Detection of mountain permafrost by combining conventional geophysical methods and thermal monitoring in the Retezat Mountains, Romania, Cold Regions Science and Technology, 119, 111-123

Onaca, A., Urdea, P., Ardelean, A., Şerban, R., 2013, Assessement of internal structure of periglacial landforms from Southern Carpathians (Romania) using dc resistivity tomography, Carpathian Journal of Earth and Environmental Sciences, 8 (2), 113-122.

Paul, P.; Bolch, T.; Briggs, K.; Kääb, A.; McMillan, M.; McNabb, R.; Nagler, T.; Nuth, C.; Rastner, P.; Strozzi, T., 2017. Error sources and guidelines for quality assessment of glacier area, elevation change, and velocity products derived from satellite data. Remote Sens. Environ. 2017, 203, 256–275.

Popescu, R., Vespremeanu-Stroe, A., Onaca, A., Cruceru, N., 2015. Permafrost in the granitic massifs of Southern Carpathians (Parâng Mountains). Zeitschrift für Geomorphologie, 59, 1, 1-20.

Rouyet, L., Eckerstorfer, M., Lauknes T. R., Riise, T., 2017. Deformasjonskartlegging rundt Longyearbyen ved bruk av satellittbasert radarinterferometri. [In Norwegian]. Rapport 13/2017. Available on: https://www.miljovernfondet.no/prosjekter/kartlegging-av-terrengstabilitet-rundt-longyearbyen/

Rouyet, L., Lauknes, T. R., Christiansen, H. H., Strand, S. M., Larsen, Y., 2019. Seasonal dynamics of a permafrost landscape, Adventdalen, Svalbard, investigated by InSAR. Remote Sens. Environ., 231, 111236, https://doi.org/10.1016/j.rse.2019.111236.

Schoeneich, P., Dall'Amico, M., Deline, P., & Zischg, A., 2011. Hazards related to permafrost and to permafrost degradation. PermaNET project, state-of-the-art report, 6.

Sing, T., Sander, O., Beerenwinkel, N., & Lengauer, T., 2005. ROCR: visualizing classifier performance in R. Bioinformatics, 21(20), 3940-3941.

Strozzi, T., Caduff, R., Jones, N., Barboux, C., Delaloye, R., Bodin, X., Kääb, A., Mätzler, E. and Schrott, L., 2020. Monitoring Rock Glacier Kinematics with Satellite Synthetic Aperture Radar. Remote Sensing, 12(3), 559, doi:10.3390/rs12030559.

Tanarro, L. M., Hoelzle, M., García, A., Ramos, M., Gruber, S., Gómez, A., ... & Palacios, D., 2001. Permafrost distribution modelling in the mountains of the Mediterranean: Corral del Veleta, Sierra Nevada, Spain. Norsk Geografisk Tidsskrift-Norwegian Journal of Geography, 55(4), 253-260.

Urdea, P., 1993. Permafrost and periglacial forms in the Romanian Carpathians. In Sixth International Conference on Permafrost, South China University of Technology Press, I (pp. 631-637).

Vespremeanu-Stroe, A., Urdea, P., Popescu, R., Vasile, M., 2012. Rock Glacier Activity in the Retezat Mountains, Southern Carpathians, Romania. Permafrost and Periglacial Processes, 23(2), 127-137.

Trombotto-Liaudat D. and Bottegal E., 2019. Recent evolution of the active layer in the Morenas Coloradas rock glacier, Central Andes, Mendoza, Argentina and its relation with kinematics. Cuad. Investig. Geográfica (doi:10.18172/cig.3946)

Westermann, S., Schuler, T.V., Gisnas, K., Etzelmuller, B., 2013. Transient thermal modeling of permafrost conditions in Southern Norway. Cryosphere, 7(2), 719-739.

Wirz, V.; Beutel, J.; Gruber, S.; Gubler, S.; Purves, R.S., 2014. Estimating velocity from noisy GPS data for investigating the temporal variability of slope movements. Nat. Hazards Earth Syst. Sci., 14, 2503–2520, doi:10.5194/nhess-14-2503-2014.

5.2 Acronyms

AD	Applicable Document
ADP	Algorithm Development Plan
ADR	Annual Displacement Rate
ATBD	Algorithm Theoretical Basis Document
AUC	Area Under the Receiver Operating Curve
B.GEOS	b.geos GmbH
BTS	Bottom Temperature of Snow Cover
CCI	Climate Change Initiative
CCN	Contract Change Notice
CR	Cardinal Requirement (as defined in [AD-1])
CRDP	Climate Research Data Package
DARD	Data Access Requirement Document
DEM	Digital Elevation Model

DGPS	Differential Global Position System
ECV	Essential Climate Variable
ERT	Electrical Resistivity Tomography
ESA	European Space Agency
ESA DUE	ESA Data User Element
E3UB	End-to-End ECV Uncertainty Budget
FDL	Frozen Debris Lobe
FPR	False Positive Rate
GAMMA	Gamma Remote Sensing AG
GCOS	Global Climate Observing System
GCP	Ground Control Points
GPS	Global Position System
GNSS	Global Navigation Satellite System
GST	Ground Surface Temperature
GTOS	Global Terrestrial Observing System
GUIO	Department of Geosciences University of Oslo
INSAR	Synthetic Aperture Radar Interferometry
IPA	International Permafrost Association
IPCC	Intergovernmental Panel on Climate Change
LOS	Line Of Sight
LST	Land Surface Temperature
MA	Moving Area
MPDM	Mountain Permafrost Distribution Model
NORCE	Norwegian Research Centre AS
NDVI	Normalized Difference Vegetation Index
PE	Permafrost Extent
PSD	Product Specifications Document
PSI	Persistent Scatter Interferometry
PVASR	Product Validation and Algorithm Selection Report
PUG	Product User Guide
PVP	Product Validation Plan
QA4EO	Quality assurance framework for earth observation
RD	Reference Document
RG	Rock Glacier
RGI	Rock Glacier Inventories
RGK	Rock Glacier Kinematic Time Series
ROMPOS	Romanian real-time positioning network
RS	Remote Sensing
RTK	Real-time kinematic
SAR	Synthetic Aperture Radar
SWE	Snow Water Equivalent
T	Temperature
TPR	True Positive Rate
UiO	University of Oslo

UNIFR	Department of Geosciences University of Fribourg
UNIS	University Centre in Svalbard
URD	Users Requirement Document
WUT	West University of Timisoara